A REVIEW OF POLISH AERONAUTICAL FATIGUE AND STRUCTURAL INTEGRITY INVESTIGATIONS DURING MAY 2023 TO APRIL 2025

Compiled by:

Dr Antoni Niepokólczycki
(antoni.niepokolczycki@gmail.com)

ICAF 2025
The 39th Conference and the 32nd Symposium of the International Committee on Aeronautical Fatigue and Structural Integrity, Xi'an, China, 9-13 June 2025

Contents

1. Load Spectra of Lightweight UAV's

(Prof. Miroslaw Rodzewicz - Warsaw University of Technology)

The foundation of fatigue testing for structural components lies in understanding the load spectra (LS) that impact these structures. With the increasing use of unmanned aerial vehicles (UAVs) in both civilian and military sectors, and their operation in airspace shared with manned aviation, the safety and reliability of UAVs have become critical. One key aspect is their fatigue durability. Research on the load spectra of both manned and unmanned aircraft has been conducted for years at the Faculty of Power and Aeronautical Engineering, Warsaw University of Technology, under the guidance of M. Rodzewicz, PhD, DSc. These efforts have resulted in numerous publications, including those in the journal Fatigue of Aircraft Structures. These publications can be accessed online, starting from the 2009 issue at https://sciendo.com/issue/FAS/2009/1 and continuing through to the 2023 issue at https://sciendo.com/issue/FAS/2022/14.

One of the applications of unmanned aerial vehicles developed at the Warsaw University of Technology is photogrammetric missions. The team led by M. Rodzewicz has significant experience in this field. A notable achievement was the use of unmanned photogrammetric aircraft for monitoring ecosystems on King George Island in Antarctica. These studies were conducted as part of the MONICA project, funded by the Polish-Norwegian POL-NOR grant. The research utilized aircraft with a classic aerodynamic layout (PW-ZOOM) as well as flying wing aircraft (Skywalker X-8) (see Fig. 1.1). During the MONICA project, it was observed that the quality of orthophotos obtained from the photographs taken by both aircraft was significantly better for the PW-ZOOM, even though identical photogrammetric systems were used in both. It was hypothesized that the observed differences resulted from the distinct dynamic behaviors during flights in turbulent conditions, which were common during photogrammetric missions in Antarctica. The encountered turbulence disrupted the flight of the PW-ZOOM aircraft less than it did the Skywalker X-8, resulting in less blurred orthophotos during flights. It is worth noting that in both aircraft, the camera was rigidly mounted in the fuselage (without a gimbal to maintain a constant angular position).

Fig. 1.1. Preparation to the take-off of PW-ZOOM (catapult) and Skywalker X8 (bungee)

Since the PW-ZOOM and Skywalker X8 aircraft responded differently to turbulence, this should be reflected in the differences in the load spectra affecting the aircraft under similar flight conditions. Therefore, detailed studies of the load spectra of both aircraft for photogrammetric missions were conducted. By utilizing the dynamic flight parameters recorded in the autopilot logs, time series of the load factor were obtained. Subsequently, the load factors n_z were converted into so-called load levels (LL) using a standard formula, and the LL time series were filtered to obtain sequences of local LL extremes. These sequences were such that if the transition between term "i" and term "i+1" involved a positive increase in LL, the subsequent transition between term "i+1" and "i+2" had to correspond to a negative increase in LL.These prepared sequences of local LL extremes were subjected to the Rainflow Counting algorithm, which allowed for the calculation of resultant load increments (resulting from the combination of a certain number of smaller LL increments). The application of the Rainflow Counting algorithm resulted in arrays of load half-cycles (Fig. 1.2).

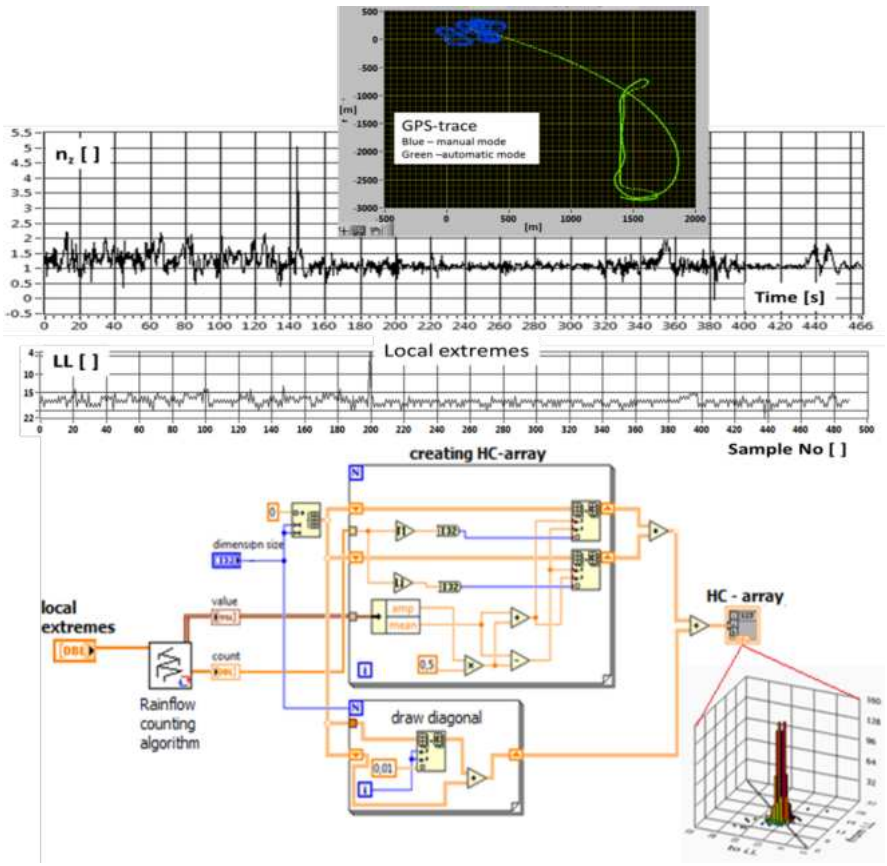

Fig. 1.2. The algorithm used for creation the half-cycle arrays implemented in the LabView

Using load half-cycle arrays from multiple flights of each of the previously mentioned aircraft, single-branch incremental load spectra were generated. On the horizontal axis of such a spectrum, the ΔLL increment values are marked, while on the vertical axis, the cumulative number of load cycles (or cumulative number of load half-cycles) is indicated. The number for ΔLL = j is the sum of the cycle counts for each ΔLL value, starting from the highest value recorded in a given flight down to ΔLL = j. The cycle counts occurring at each ΔLL level are referred to as level-specific load cycle numbers.

The numbers of load cycles related to flight time were subject to further statistical analysis, which included examining the maximum value, average value, and standard deviation. Based on this, new forms of incremental load spectra were developed for the flight session, covering all analyzed flights. These new forms include the load spectrum envelope (LS envelope), which contains extreme values of the number of cycles per hour of flight that occurred at various ΔLL levels during all flights in the session; the aggregated load spectrum (aggregated LS), which includes averaged load cycle numbers (calculated as the sum of load cycles divided by the total flight time of the session); and the weighted load cycle envelope (weighted LS

envelope), which contains extreme values of the number of cycles per hour of flight at various ΔLL levels, multiplied by weights that are the ratio of the sum of flight times with non-zero numbers at the analyzed ΔLL level to the total flight time of the session.These incremental load spectra for the entire measurement session range from extremely conservative (LS envelope) to semi-conservative (weighted LS envelope) and non-conservative (aggregated LS). The degree of conservatism of the load spectrum affects the estimated fatigue life and the risk of underestimation. It was demonstrated that if fatigue calculations were conducted for a selected critical load-bearing structure element (e.g., an aluminum alloy wing connector) using the fatigue spectrum of the PW-ZOOM aircraft or the Skywalker X8 aircraft, the differences in results would be several hundred percent in favor of the PW-ZOOM aircraft, which reacts calmly to turbulence. Details of all these calculations are provided in the paper:

Rodzewicz Mirosław, Dominik Głowacki, and Jarosław Hajduk. 2022. *„Comparative Analysis of the Load Spectra Recorded during Photogrammetric Missions of Lightweight UAVs in Tailless and Conventional Configurations”*. Fatigue of Aircraft Structures 2022: 114–34. https://doi.org/10.2478/fas-2022-0009

Below is a chart from the article illustrating the differences in load spectra between the PW-ZOOM and Skywalker X-8 aircraft during a photogrammetric mission (Fig. 1.3). Symbol n_1hC means here: cumulative number of load cycles per 1h.

It is worth noting that despite significant differences in load spectra and variations in the quality of orthophotographs, the dynamic behavior of either aircraft, when observed from 300 meters above the ground in identical atmospheric conditions, appears to be quite similar. The research presented in the aforementioned article demonstrates the usefulness of fatigue analysis tools in assessing the suitability of unmanned aircraft for photogrammetric missions by showing the load spectrum generated during such missions under specific turbulence conditions.

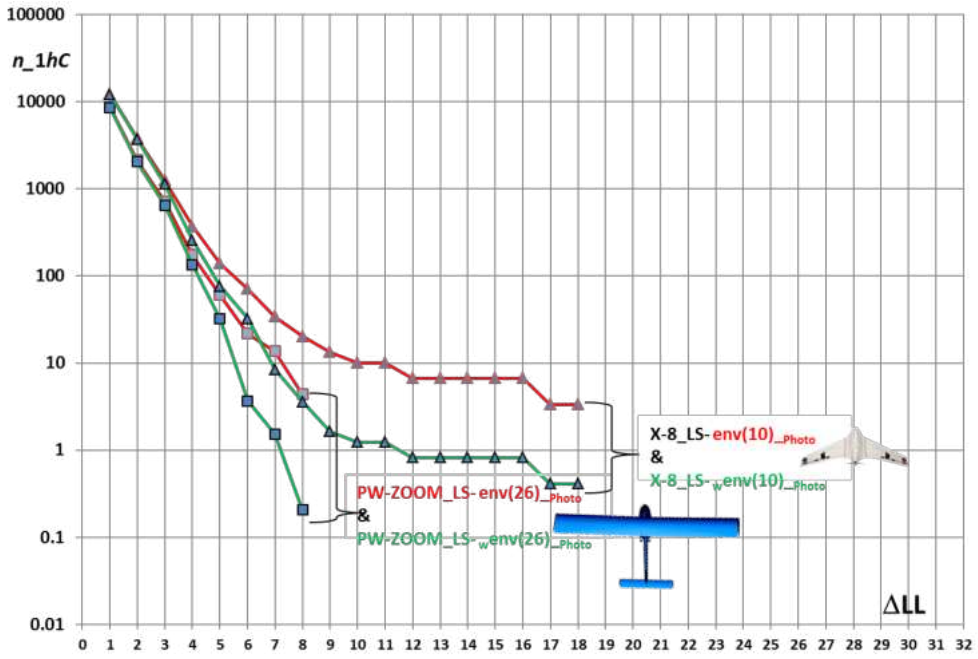

Fig. 1.3. The incremental load spectra (LS envelope and LS weighted envelope) for photogrammetric part of the flight mission.

Contact: Prof. Miroslaw Rodzewicz - Miroslaw.Rodzewicz@pw.edu.pl

2. NDT and SHM Techniques for Evaluation and Prediction of Condition and Residual Strength of Aircraft Structures

(Prof. Andrzej Katunin - Silesian University of Technology)

One of the key challenges in the aerospace industry is predicting the residual strength of composite structures following impact damage. Traditional destructive testing methods, such as Compression After Impact (CAI), have limitations in practical applications due to cost and complexity. In the performed studies, the hybrid methodology combining non-destructive testing (NDT) techniques with numerical modeling to improve accuracy and efficiency has been proposed [1]. This methodology integrates ultrasonic C-scans with finite element modeling to evaluate impact-induced damage and structural residual life of composite materials. This method enables a more precise assessment of structural integrity and damage propagation, taking into consideration its shape acquired directly from NDT

inspections. The developed parametric models allowed predicting geometrical properties of impact damage and resulting residual life in composite structures in a certain range of impact energies. They can be imported to finite element software for further evaluation of structural residual life. Such parametric models, besides the necessity of individual tuning for the specific problem, provide a solution for evaluation of a residual life of composite structures after impact.

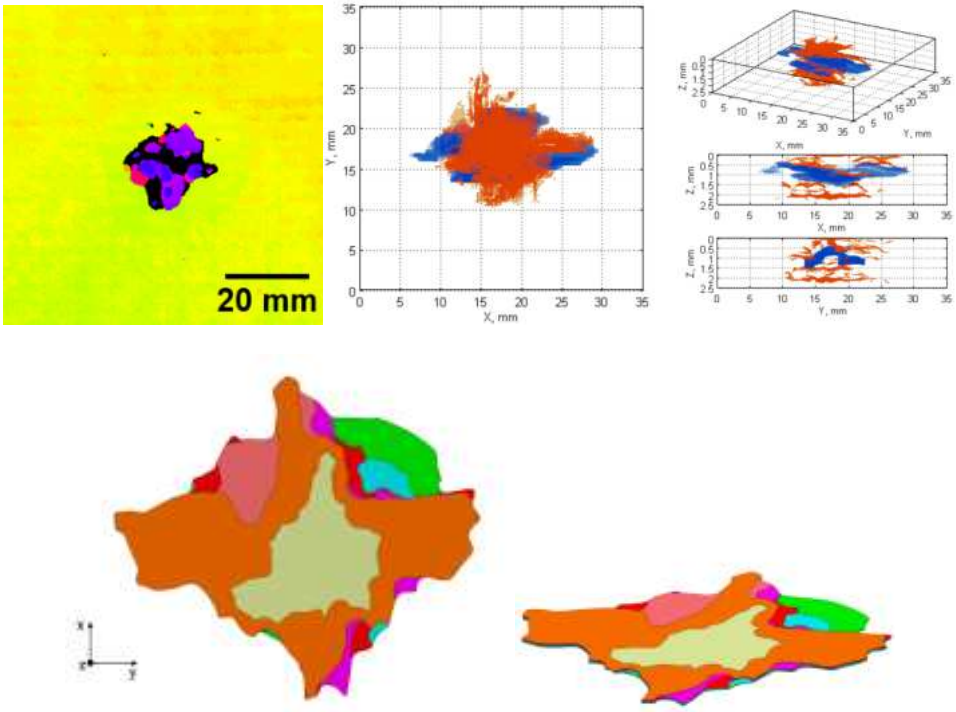

Fig. 2.1. C-Scan, reconstruction, and parametrized CAD model of an impact damage of a composite structure (adapted from [1]).

Corrosion remains a significant concern in aircraft maintenance, particularly in metallic fuselage components. Early detection and monitoring of corrosion are crucial for maintaining the structural integrity of aging aircraft and preventing catastrophic failures. Non-destructive evaluation (NDE) techniques, such as the D-Sight method, have been developed to improve the detection and quantification of hidden corrosion, which is one of the most difficult types of corrosion to detect. Our recent activities were focused on improving D-Sight technique by implementing advanced processing of D-Sight images towards automation and quantification of hidden corrosion.

In our studies [2], we introduced an automated technique using D-Sight image processing for hidden corrosion quantification, and tested it on D-Sight images from inspection of military helicopters. We also took our efforts for monitoring of hidden

corrosion growth in aircraft structures [3]. These approaches utilize historical image data to track corrosion progression over time, improving predictive maintenance strategies. The ability to automatically quantify and track corrosion allows for more proactive maintenance planning and resource allocation, ensuring that interventions are performed before structural degradation reaches critical levels.

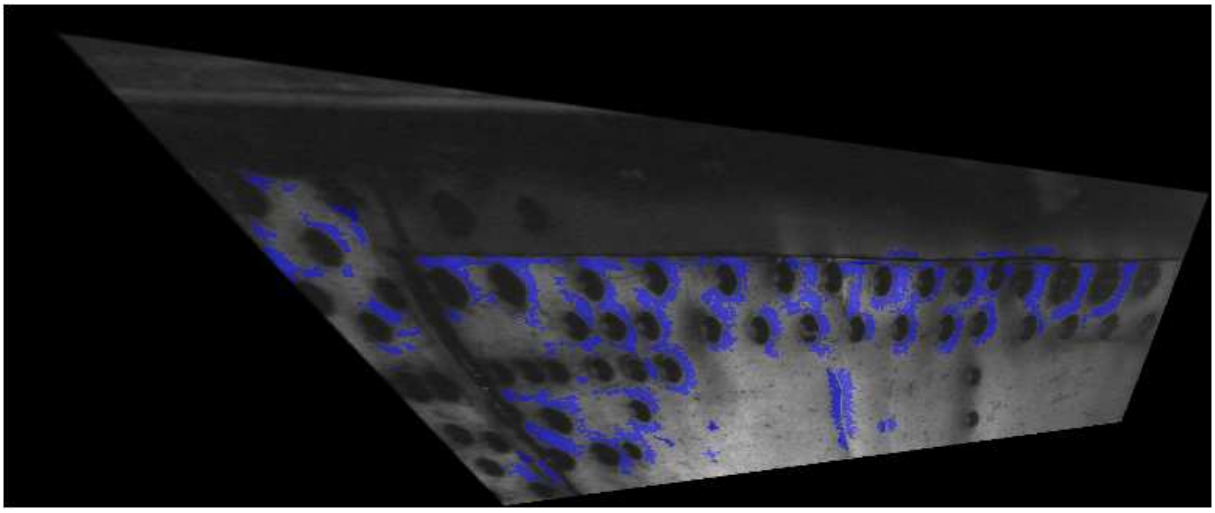

Fig. 2.2. The exemplary result of detection of hidden corrosion on an aircraft fuselage panel using the developed algorithm [2].

Additionally, we proposed a method combining D-Sight inspections with finite element modeling to assess corrosion depth and severity [4]. This hybrid approach enhances the accuracy of structural assessments and aids in maintenance decision-making by providing a more comprehensive understanding of material degradation. These findings demonstrated that combining D-Sight imaging with numerical simulations allowed for the detection of corrosion at earlier stages compared to traditional ultrasonic and radiographic inspections.

Within our activities in non-destructive evaluation we continue developing our authored NDT technique, the self-heating based vibrothermography (SHVT). In our recent study [5], we explored SHVT to assess damage in composite plates. This technique, operating under resonant frequency mechanical excitation, provides real-time damage detection through thermal imaging, being a solution for one-sided access to inspected structures as well as inability of using external heat sources for excitation as in the classical thermographic techniques. The study highlighted that SHVT can identify damage with high sensitivity, making it particularly useful for high-performance aerospace composites.

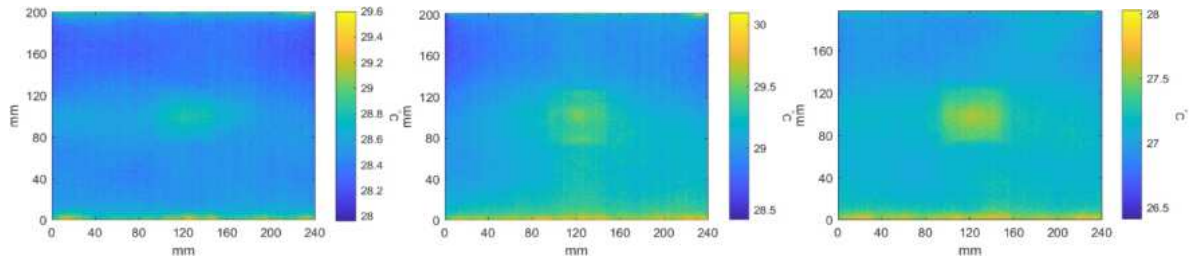

Fig. 2.3. The exemplary results of identification of an artificial damage in GFRP plates using SHVT non-destructive technique: (a) 10%, (b) 25%, and (c) 50% of thickness reduction.

We also took our efforts in developing and adjusting eddy current testing (ECT) technique for inspection of carbon fiber-reinforced composites (CFRP). In our recent study [6], we investigated eddy current pot-core sensors for detecting subsurface damage in CFRP structures. These findings highlight the advantages of eddy current testing (ECT) over traditional ultrasonic techniques for detecting barely visible impact damage (BVID). The study demonstrates that ECT offers increased sensitivity to certain types of defects, which are often missed by other NDT methods. It was demonstrated that specific coil geometries and excitation frequencies significantly influence detection accuracy, providing a framework for sensor optimization.

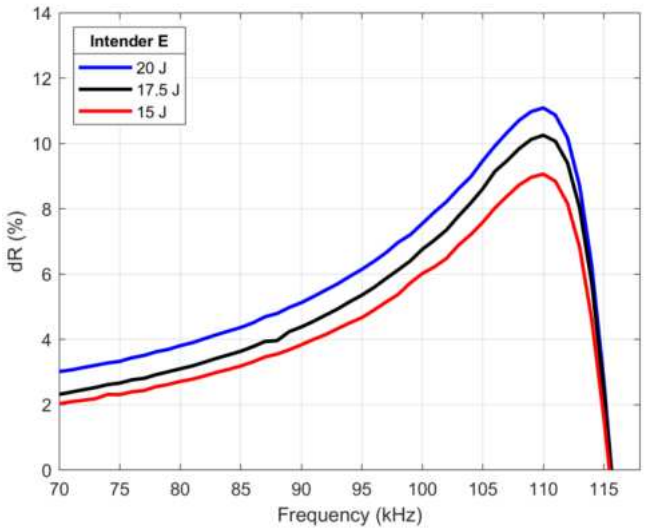

Fig. 2.4. Distinguishability of impact damage in CFRP specimens for various impact energies using the developed ECT probe [6].

Furthermore, common activities of the Structural Integrity Assessment Research Group of the Silesian University of Technology and the Division of Airworthiness of the Air Force Institute of Technology resulted in development mobile robotic platform to automate NDT inspections. The developed robotized mobile platform equipped with eddy current probes for aircraft inspections was described in [7]. This system enhances efficiency by automating labor-intensive scanning processes and reducing human error. The use of robotic systems in NDT inspections significantly accelerates data collection and enhances consistency in damage detection. It is expected that automated inspection systems can reduce inspection times by up to 40% while maintaining high detection accuracy.

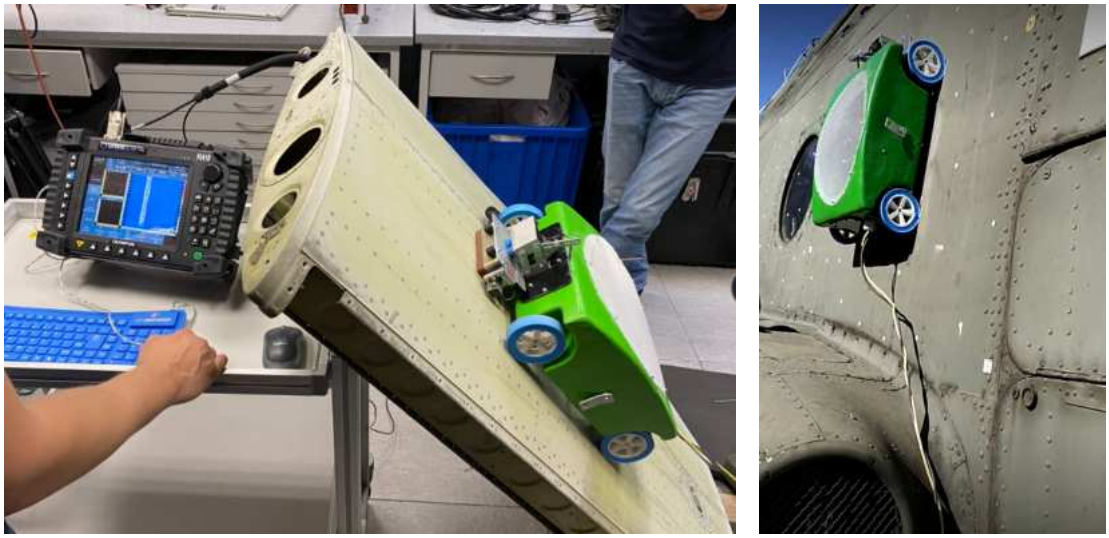

(a) (b)

Fig. 2.5. Testing of the developed mobile robotic platform in laboratory conditions and on the fuselage of a military helicopter.

The integration of advanced sensor networks into SHM systems is crucial for real-time damage monitoring and predictive maintenance. Several studies focus on optimizing sensor placement to enhance detection efficiency while minimizing costs. Effective sensor placement ensures accurate data collection while reducing redundancy and costs associated with maintenance operations. Our activities were focused on optimal sensor placement (OSP) for modal-based SHM systems that were tested on composite structures.

In our study [8], we investigated modal-based SHM techniques for composite structures, demonstrating the effectiveness of machine learning algorithms in damage classification. The incorporation of machine learning models allows for automated

data interpretation and improved damage detection efficiency, reducing the need for manual inspection and analysis in the conditions of limited number of sensors and other physical limitations. The developed methodology was successfully validated experimentally on CFRP panels [9]. In the recent study [10], we employed a genetic multi-objective optimization algorithm (NSGA-II) to optimize sensor placement in composite structures. This approach balances detection accuracy with the number of required sensors, improving SHM system performance and reliability. The study highlighted that optimizing sensor locations not only enhances damage detection but also reduces false alarms, improving maintenance efficiency.

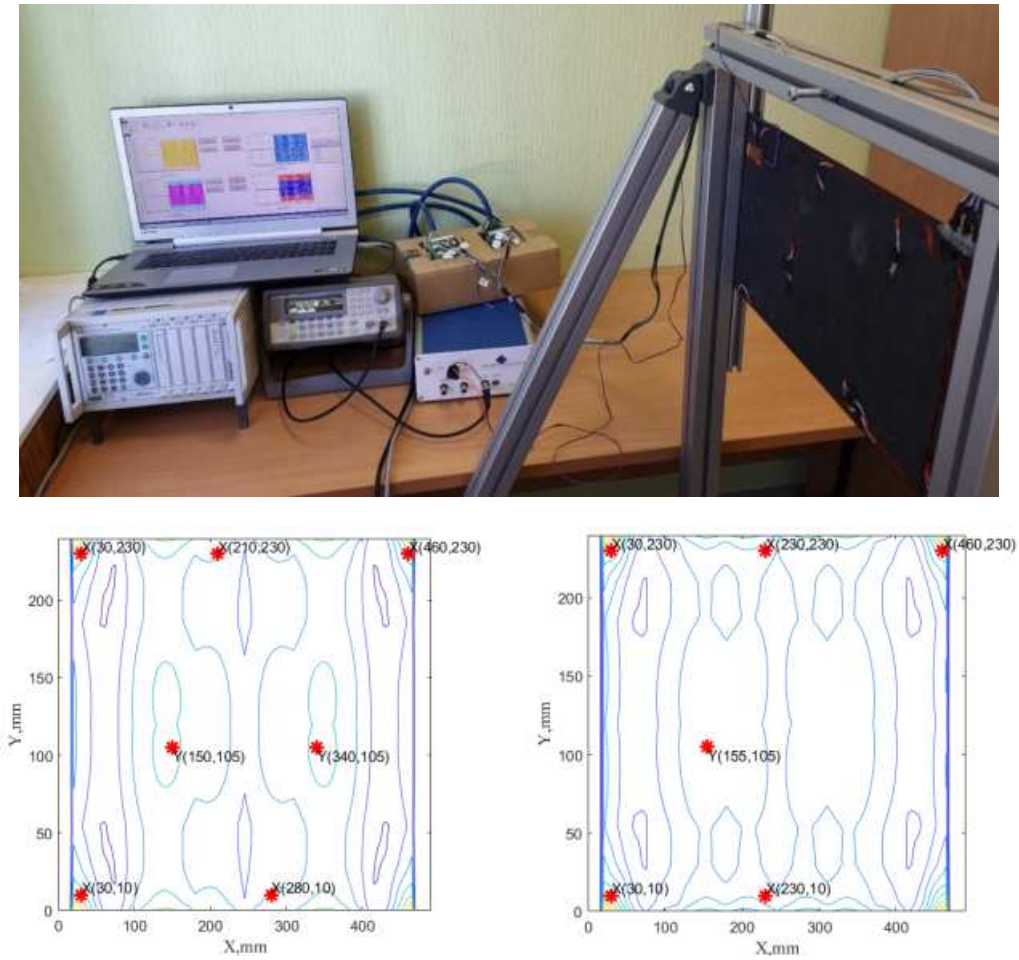

Fig. 2.6. The experimental setup [8] and exemplary optimal sensor placement [10] for the investigated SHM problem.

These developments align with industry trends emphasizing predictive maintenance, reduced operational costs, and improved aircraft safety. Future research would focus on further integrating machine learning and artificial intelligence into NDT and SHM frameworks to enhance automation and predictive capabilities. The

combination of these advanced methodologies ensures more efficient aircraft maintenance strategies, minimizing risks and maximizing operational longevity.

Fatigue of composite structures at appearance of the self-heating effect

The self-heating effect in polymer-matrix composites (PMCs) subjected to fatigue loading is a critical factor influencing their structural integrity and service life. Recent studies have explored numerical modeling, experimental validation, and new methodologies to assess and mitigate damage accumulation induced by self-heating. Over the last years our studies in this thematic area were focused on fatigue evaluation and prediction in PMCs, self-heating behavior characterization in various frequency ranges, and structural durability improvements by limitation of the self-heating effect during fatigue.

In [11], we conducted an extensive review on mitigating fatigue damage caused by self-heating in PMCs. This study emphasized cooling techniques, material selection strategies, and hybrid composite designs to minimize thermal degradation. It was concluded that improving thermal conductivity and implementing active cooling solutions can significantly extend the fatigue life of composite structures, particularly in high-stress applications such as aerospace and wind turbine components.

We have also investigated the self-heating effect in hybrid bio-composites, demonstrating that critical self-heating temperature can serve as an alternative fatigue limit indicator [12]. In this research study, we analyzed flax, glass/flax, Kevlar/flax, and carbon/flax composites, revealing that hybridization can enhance fatigue resistance. Acoustic emission monitoring and microscopic characterization provided additional insights into fracture mechanisms, showing that self-heating-induced degradation differs depending on fiber composition and matrix interactions.

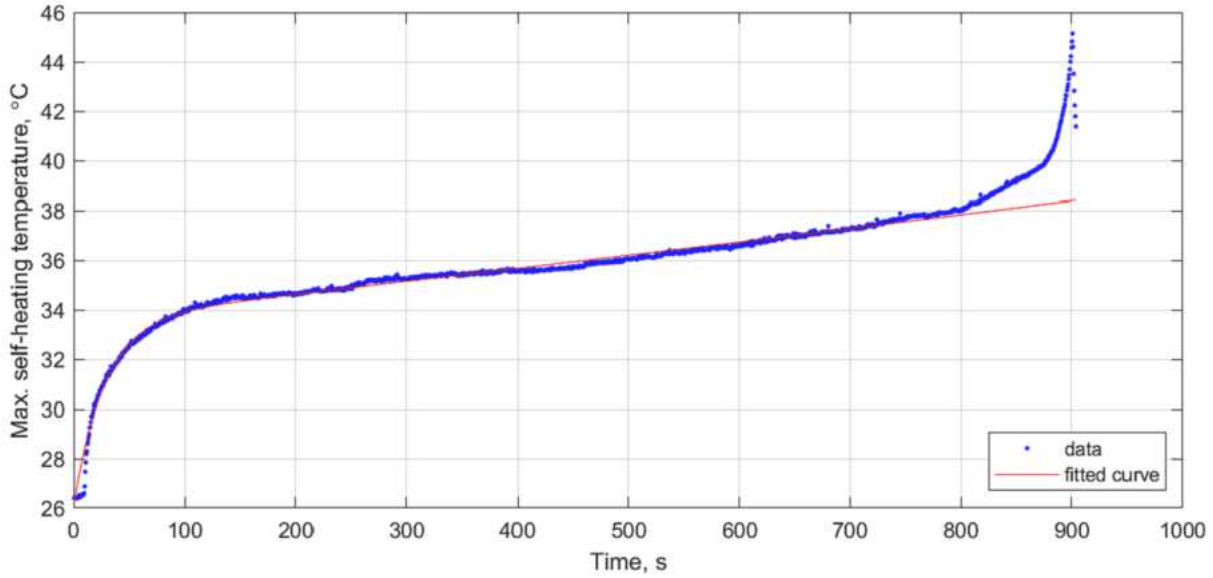

Fig. 2.7. An exemplary self-heating temperature history curve with fitting curve for a Kevlar/flax hybrid composite demonstrating the exceeding of the critical self-heating temperature (understood as between self-heating temperature curve and fitting model) [12].

Common studies with the University of Freiburg were focused on fatigue strength estimation of CF/PEKK composites through self-heating temperature analysis using high-frequency cyclic bending tests [13,14]. It was demonstrated that fatigue strength can be reliably estimated through temperature evolution patterns, providing a rapid and efficient alternative to traditional fatigue life assessment methods. This research also highlighted the significance of distinguishing between stationary and non-stationary self-heating regimes, as the latter leads to accelerated degradation and thermal fatigue failure. Further, we expanded on these findings by investigating thermomechanical fatigue behavior of CF/PEKK composites under low and ultrasonic frequencies. This study combined experimental approaches to construct S-N curves for different loading regimes, revealing that heat dissipation rate can serve as a linking parameter between low-frequency and high-frequency fatigue tests. Fractography confirmed similarities in fatigue damage mechanisms across different loading conditions, supporting the feasibility of cross-regime fatigue life predictions.

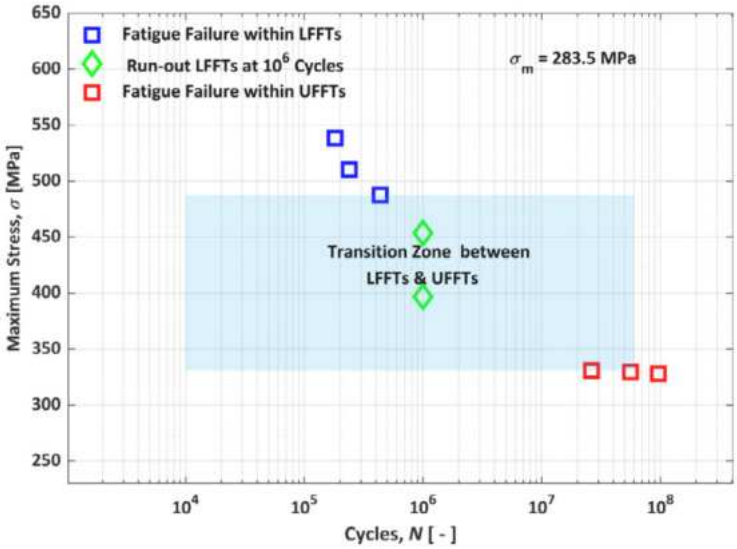

Fig. 2.8. A combination of low-frequency and ultrasonic-frequency fatigue responses for CF/PEKK thermoplastic composite indicating the transition zone between traditional and accelerated fatigue testing techniques [14].

Our recent contribution is the study, which integrates numerical simulations with experimental validation to model self-heating effects in PMCs under low-cycle fatigue conditions [15]. These findings demonstrate that radiative heat flux must be considered to accurately predict self-heating temperatures, and that temperature variations remain negligible across the thickness of PMC specimens. Additionally, a temperature-stress approach that correlates applied stress amplitudes with thermal response has been introduced, allowing for improved fatigue life prediction based on residual flexural stiffness.

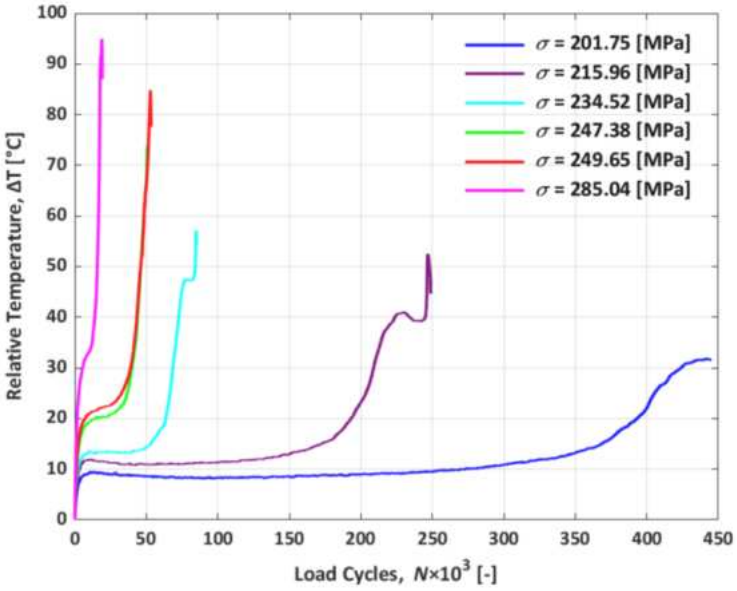

Fig. 2.9. The self-heating temperature history curves for various stress levels indicating the influence of the self-heating effect on fatigue durability of GFRP composites [15].

These findings contribute to a more comprehensive understanding of the self-heating phenomenon in fatigue-loaded composite structures. Future research will focus on further integrating machine learning for predictive modeling, refining hybrid composite formulations, and developing real-time monitoring systems to optimize structural performance and durability.

References

1. Katunin A., Danek W., Wronkowicz A., Dragan K., *Methodology of residual strength prediction of composite structures with low-velocity impact damage based on NDT inspections and numerical-experimental CAI testing,* International Journal of Impact Engineering 181, 2023, 104762.
2. Katunin A., Synaszko P., Dragan K., *Automated identification of hidden corrosion based on the D-sight technique: A case study on a military helicopter,* Sensors 23, 2023, 7131.
3. Katunin A., Nagode M., Oman S., Cholewa A., Dragan K., *Monitoring of hidden corrosion growth in aircraft structures based on D-Sight inspections and image processing,* Sensors 22, 2022, 7616.
4. Katunin A., Lis K., Joszko K., Żak P., Dragan K., *Quantification of hidden corrosion in aircraft structures using enhanced D-Sight NDT technique,* Measurement 216, 2023, 112997.
5. Amraei J., Katunin A., Wachla D., Lis K., *Damage assessment in composite plates using extended non-destructive self-heating based vibrothermography technique,* Measurement 241, 2025, 115670.
6. Tytko G., Rogala T., Katunin A., Yin W., *Damage detection in carbon fiber-reinforced composite structures using eddy current pot-core sensor,* IEEE Access 12, 2024, 123609-123620.
7. Toman R., Rogala T., Synaszko P., Katunin A., *Robotized mobile platform for non-destructive inspection of aircraft structures,* Applied Sciences 14, 2024, 10148.

8. Ručevskis S., Rogala T., Katunin A., *Optimal sensor placement for modal-based health monitoring of a composite structure,* Sensors 22, 2022, 3867.

9. Ručevskis S., Rogala T., Katunin A., *Monitoring of damage in composite structures using an optimized sensor network: A data-driven experimental approach,* Sensors 23, 2023, 2290.

10. Rogala T., Ścieszka M., Katunin A., Ručevskis S., *Genetic multi-objective optimization of sensor placement for SHM of composite structures,* Applied Sciences 14(1), 2024, 456.

11. Amraei J., Katunin A., *Recent advances in limiting fatigue damage accumulation induced by self-heating in polymer-matrix composites,* Polymers 14, 2022, 5384.

12. Katunin A., Wachla D., Santos P., Reis P.N.B., *Fatigue life assessment of hybrid bio-composites based on self-heating temperature,* Composite Structures 304, 2023, 116456.

13. Premanand A., Rogala T., Wachla D., Amraei J., Katunin A., Khatri B., Rienks M., Balle F., *Fatigue strength estimation of a CF/PEKK composite through self-heating temperature analysis using cyclic bending tests at 20 kHz,* Composites Science and Technology 243, 2023, 110218.

14. Amraei J., Rogala T., Katunin A., Premanand A., Kokot G., Wachla D., Kuś W., Bilewicz M., Khatri B., Balle F., *Thermomechanical fatigue behavior of CF/PEKK composite under low and ultrasonic frequencies,* Composites Part B: Engineering 281, 2024, 111539.

15. Amraei J., Katunin A., Lipińska M., *Numerical simulation and experimental validation of self-heating of polymer-matrix composites during low-cycle fatigue loading,* International Journal of Fatigue 188, 2024, 108510.

Contact: Prof. Andrzej Katunin - Andrzej.Katunin@polsl.pl

3. Structural Health and Ballistic Impact Monitoring and Prognosis on a Military Helicopter (SAMAS 2)

A. Kurnyta [a)], M. Dziendzikowski [a)], K. Kowalczyk [a)], W. Majda [b)], J. Chojnacki [b)], M. Kozera [c)], K. Dragan [a)], M. Kurdelski [a)]

SAMAS2 is a cat. B European Defence Agency project within the consortium members consists of representatives of 2 coutries:

- Poland: Air Force Institute of Technology [a)], Military Aviation Works No. 1 in Łódź [b)], Łukasiewicz Research Network – Institute of Aviation [c)], Military University of Technology [d)];
- Italy: Politecnico di Milano - Dipartimento di Meccanica (consortium Leader), Leonardo Helicopters, Consiglio Nazionale delle Ricerche CNR-ICMATE.

The overall aim of SAMAS 2 project within the consortium is to develop a Structural Health Monitoring and Prognosis (SHMP) tool for corrosion degradation, bullet impact damages, that can be even possibly exploited for airframe load monitoring and generic damage development. These have been identified as critical factors for the structural integrity of the helicopter, since they can compromise the whole structural assessment and be a safety concern for the crew. Intermediate activities include, among others the verification if fault-tolerant design can be extend to corrosion, developing the effective methods of monitoring corrosion, airframe loads and damages, extensive on-ground and in-flight tests of elaborated diagnostic system to increase its TRL.

Polish side activities are mainly devoted to verification of selected corrosion, load and damage monitoring sensor technologies due to extract relevant damage features from sensors' signal and to provide both the actual healthy condition of the helicopter components as well as to detect the damage progression. On ground research tasks for corrosion consisted of conducting corrosion damage growth tests using piezoelectric and eddy current sensors in the defect monitoring process. The development of the corrosion defect was performed in an electrochemical process (Figure 3.1).

In terms of monitoring the helicopter transmission damage, a stand was developed and built based on the system of a real helicopter. The system consisted of the drive, the main gearbox with the mass equivalent of the blades, the hanger bearings for the shaft and the final gear. Tests were carried out consisting of many scenarios, introducing simulated damages and recording the response of the system from vibration sensors. The collected database allowed the development of

algorithms for analyzing data and symptoms of damage originating from the shaft and rear rotor imbalance, shaft skewing, bearing seizure (Figure 3.2).

The final step within the project is a preparation of the in-flight test prototype for a comprehensive evaluation system for the structure and selected critical helicopter systems in order to increase safety and reduce the operating costs of the helicopter. The system performance consisted of the integrated network of sensors of different types, connected to a additional on-board data recorder will be evaluated within real operational conditions. Experimentally, realistic sensor fluctuations will be captured, which can provide an input for a new assessment of the algorithm performances. Those data will be used to evaluate the effectiveness of the SHMP system in a more realistic environment and the capability to monitor damage and distinguish damage features from external confounding influences.

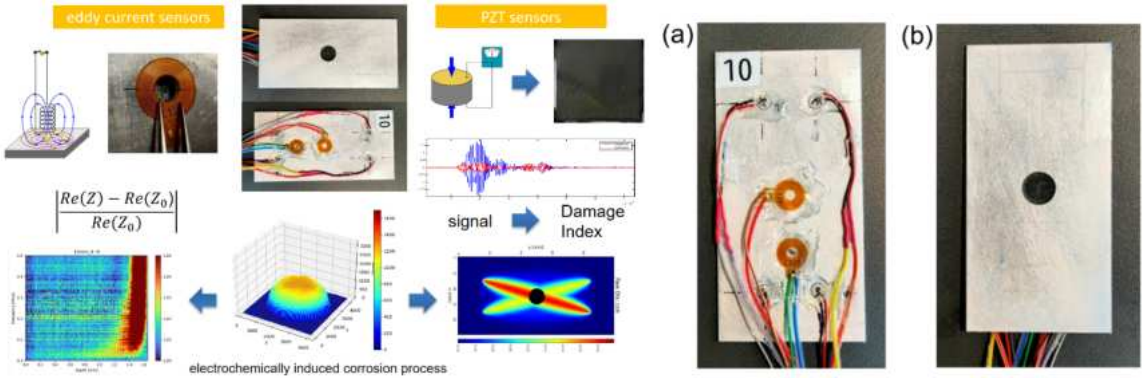

Figure 3.1. Corrosion monitoring techniques evaluation based on PZT and ECS sensors

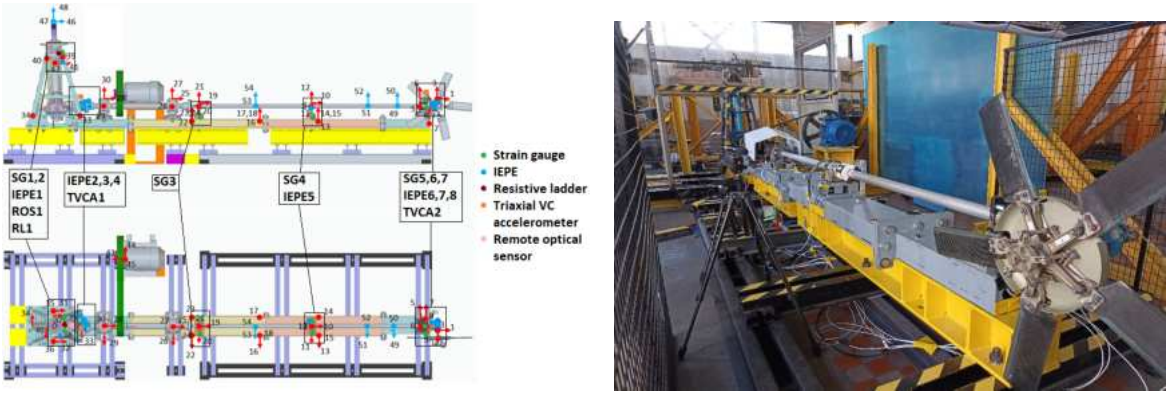

Figure 3.2. Test rig for helicopter transmission monitoring

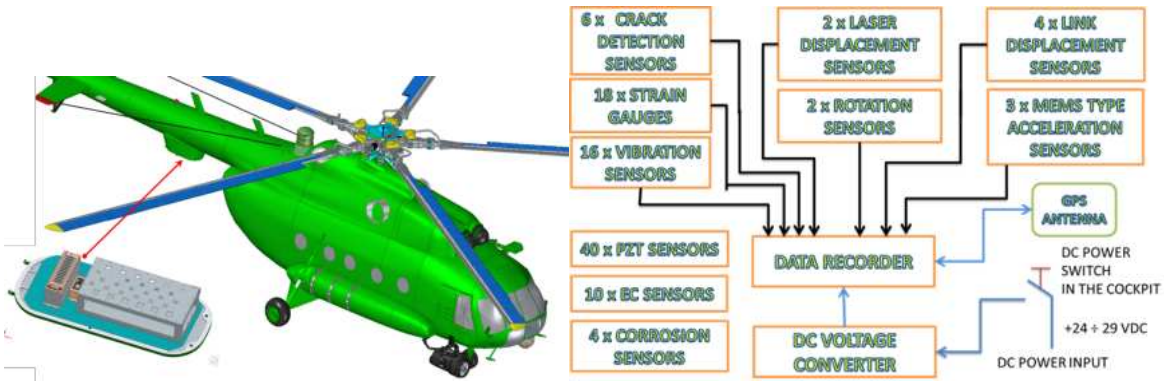

Figure 3.3. In-flight test system configuration and diagram

Contact: Prof. Krzysztof Dragan - krzysztof.dragan@itwl.pl

4. Crack Propagation Tests for Load Sequences Developed using Different Flight Parameters

(Piotr Reymer [1,2] , Kamil Kowalczyk [1] , Marta Baran [1] , Dominik Nowakowski [1] , Michał Dziendzikowski [1] , Andrzej Leski [2,3]

[1] Air Force Institute of Technology, Warsaw, Poland

[2] Military University of Technology, Warsaw, Poland

[3] Lukasiewicz Research Network – Institute of Aviation, Warsaw, Poland)

Introduction

Military aircraft loads are highly variable and hard to predict in comparison to the commercial aviation due to the versatile missions carried out with various armament and the individual approach of each military pilot. This makes it much more complicated to define actual loads exerted on the structure without direct in flight measurements as well as to estimate load sequences in case of data loss due to onboard Flight Data Recorder (FDR) malfunction or data mishandling. On the other hand instrumenting all the aircraft in the fleet with direct load measuring sensors and necessary recording equipment is hard to justify from a financial point of view.

The goal of the research was to investigate the possibility to define load spectra for the PZL-130 “Orlik” TC-II turbopiston propeller military trainer aircraft based on available flight parameters recorded during regular operation with the onboard FDR and compare the crack propagation potential of these spectra to the load spectrum

obtained from direct strain measurement of the lower wing spar during a Operational Load Monitoring program (OLM).

Flight data acquisition and initial analysis

Data used for load sequences preparation were recorded during the OLM program carried out during Service Life Extension Program of the PZL-130 "Orlik" TC-II aircraft (SLEP). The OLM was focused on capturing the real strain signals from over 100 strain gauges installed on the aircraft structure simultaneously to actual flight data recorded by the onboard FDR. These data were therefore used for definition of load sequence for the Full Scale Fatigue Test (FSFT) of the structure [10]. Figure 4.1 shows the overall strain gauge array on the PZL-130 aircraft structure during OLM.

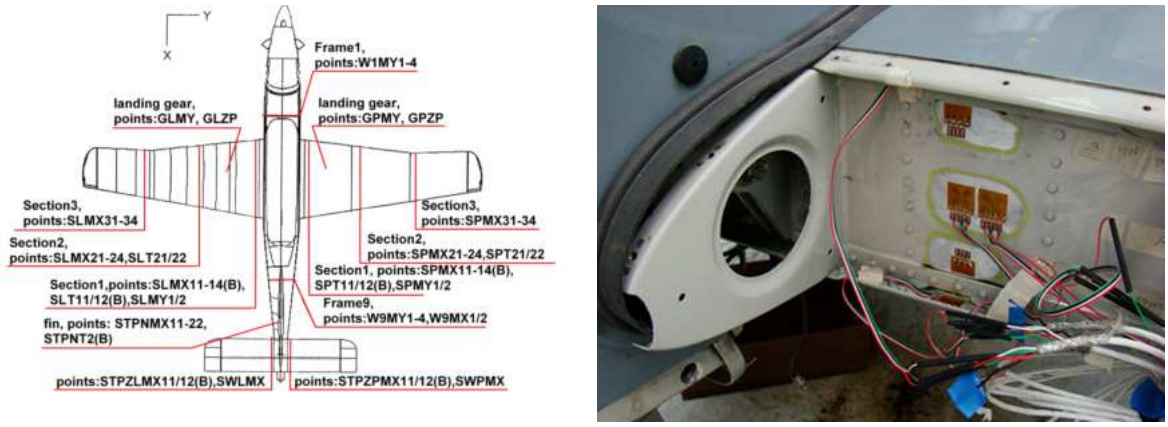

Figure 4.1. Location of strain gauges during the OLM and the SLM14 sensor

Since the direct measurement of strain state during flight gives the overall information of the load state in the element regardless of the actual load condition [11-12], therefore the comparative load spectrum used in this research was based on the *SLMX14* strain gage signal, which was installed on the lower flange of PZL-130 aircraft (Fig. 4.1). The strain gauge was a T-rosette half bridge which allowed for temperature compensation (crucial for measurements on a structure operated in variable ambient temperature) and resulted with elevated sensitivity ($1+\nu$, where ν is the Poisson's ratio of the material) [4-6]. Other available flight parameters recorded by the onboard FDR were:

- load factor – n_z [-],
- horizontal speed – V_p [km/h],
- barometric height – H_b [m],
- horizontal stabilizer angle – dh [°],

- flaps extension – *dkl* [%],
- ailerons angle - *dl* [°],
- vertical stabilizer angle - *dv* [°].

The OLM was divided into three phases, in which firstly the aircraft carried out planned flights in order to capture strains corresponding to particular exercises and maneuvers, secondly the aircraft was operated according to standard training plan and finally the measurement system was reduced leaving 8 strain gauges (4 on wings including *SLMX14*) and the aircraft continued regular flights.

Throughout these three stages 350 records were gathered, among which two were defined as ground tests and 1 duplicate record was found, which gave total of 347 flights with various intensity (considered as maximum load factor range in a flight), height and speed of flight.

Further data analysis revealed, that 29 records had damaged nz signals (8,4% of all data, however *SLMX14* signal was intact and fully usable). In order both to validate the gathered data by defining any discrepancies which might be caused by a malfunction of the sensors or recording equipment the physical thresholds of the signals were determined:

- load factor: from -2 to 7,
- SLMX14 strain gauge: from 0 to 2100 μStr,
- Barometric height: from 0 to 10 000 m,
- Horizontal speed: from 0 to 440 km/h.

Similarly the characteristic values of *SLMX14* strain gauge in defined flight states:

- on ground - 60 μStr,
- level flight with n_z =1 - 320 μStr.

In the preliminary assumptions the flight data were to be extracted from overall records basing on the weight on wheels signal. However due to unreliable values of this sensor the were determined basing on the change of air speed and height. The following values were used:

- take off – V_p>100 km/h, H_b>300m,
- landing – V_p<100 km/h, H_b<300m.

Defined thresholds allowed to prepare the gathered data for further analysis and load sequences definition.

Load sequences definition

After the initial verification the gathered data were analyzed in order to find correlations between individual parameters. The initial correlation matrix for the

available parameters is shown in Table 4.1. Since the *SLMX14* strain signal is considered to be the parameter most reliably corresponding with the actual tensile strain state in the lower spar correlations of all the other parameters to *SLMX14* ware considered. As mentioned before the load factor, therefore indirectly the lift force, is considered the main driver for wing load therefore resulting in the highest 0.93 correlation coefficient with the strain value. Secondly the horizontal speed V_p and flight height H_b did show noticeable correlation with the stain signal, resulting in 0.61 and 0.43 correlation factors respectively.

The control surfaces deflection parameters did not show clear linear correlation with neither the SLMX14 nor the load factor therefore were not taken into consideration in this analysis. Using more complicated flight mechanics dependencies might result in more usable correlations between the parameters, however this is beyond scope of the presented analysis.

Table 4.1. Correlation matrix for the available flight parameters

Variable	**SLMX14**	**n_z**	**H_b**	**V_p**	**dh**	**dkl**	**dl**	**dv**
SLMX14	1.00	0.93	0.43	0.61	0.37	-0.30	-0.03	-0.07
n_z	0.93	1.00	0.29	0.39	0.28	-0.14	-0.08	-0.03
H_b	0.43	0.29	1.00	0.30	0.42	-0.49	0.09	0.17
V_p	0.61	0.39	0.30	1.00	0.22	-0.46	-0.08	-0.15
dh	0.37	0.28	0.42	0.22	1.00	0.08	-0.04	0.22
dkl	-0.30	-0.14	-0.49	-0.46	0.08	1.00	-0.00	0.15
dl	-0.03	-0.08	0.09	-0.08	-0.04	-0.00	1.00	-0.15
dv	-0.07	-0.03	0.17	-0.15	0.22	0.15	-0.15	1.00

Therefore the load sequence definitions were based on these four parameters: strain value *SLMX14*, load factor n_z, horizontal speed V_p, and barometric height H_b. Since the *SLMX14* strain signal was considered as the most accurate measure of the actual strain state of the structure and moreover it is not available in the regular FDR data from operation (it was only available for the data recorded during the OLM program) it was decided to define the comparative load sequence based on the *SLMX14* signal from all of the flights. Additionally the remaining parameters, which are recorded during regular operation, will be used to define three types of load spectra, each more complex than the previous one.

The first spectrum would use only the load factor n_z, whereas the second the load factor n_z and the barometric height H_b and finally the third one all the previously

mentioned parameters and horizontal velocity V_p. Linear regression analysis defining the values of *SLMX14* using the above defined sets of parameters was carried out in STATISTICA software resulting in linear regression models which parameters are shown in Table 4.2.

Table 4.2. Linear regression models parameters for the SLMX14 equations using flight parameters

Independent variables	**R**	**R^2**	free coefficient	**a**	**b**	**c**
n_z	0.9320	0.8686	-64.1018	388.8242	-	-
n_z , H_b	0.9459	0.8947	-113.747	368.296	0.046	-
n_z , H_b, V_p	0.9742	0.9491	-231.156	332.524	0.032	0.726

As can be observed from the presented values, the addition of H_b and further on V_p does increase the overall coefficients of determination of the consecutive models. These relatively small differences in representation of a single value of *SLMX14* will supposedly have a larger impact when the total fatigue life of a specimen is considered, what is the definitive goal of the presented research.

In order to both prepare the spectra for the presented research and to be able to create spectra based on current flight data, a dedicated software was created. The software allowed for automated flight data processing by definition of flight states based on before mentioned criteria, selection of desired regression model and other parameters like low bypass filtration. Moreover in order to enable comparison of the test results obtained for each of the four spectra the load cycles in each sequence corresponded to so called Simulated Flight Hours (SFH), which means that execution of a certain part of each sequence was considered to represent the defined number of flight hours of the PZL-130 aircraft. The number of cycles and corresponding SFH for each sequence are given in Table 4.3.

Table 4.3. Load sequences characteristics

Sequence	**SLMX14**	**n_z**	**n_z+Hb**	**n_z+Hb+Vp**
Number of cycles	52894	30434	28241	25348
SFH	270.6	266.7	267.7	271

Each spectrum was filtered with a 5% low bypass filter in order to speed up the laboratory tests, and furthermore due to requirements of the standard [13] and potential problems with transitions from negative to positive values all low values were truncated below 100 N.

Test preparation and execution

Crack propagation tests using the obtained spectra were carried on CT samples designed according to the standard [13]. The overall sample dimensions are shown in Figure 4.2 and are given in Table 4.4. Samples were placed in specially designed clamps according to standard requirements and loaded in tension on electromechanical MTS Acumen 12T strength testing machine using the prepared load sequences (Fig 4.3).

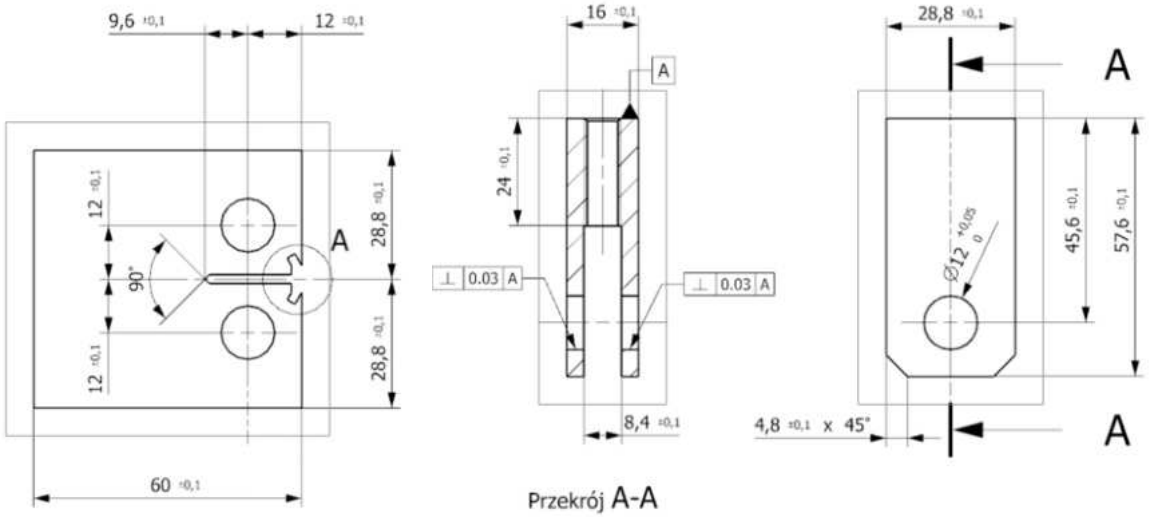

Figure 4.2. Technical drawing of the CT samples used in the test and the mount

Table 4.4. Dimensions of the CT specimens used in the test

W [mm]	B [mm]	Width [mm]	Height [mm]	Holes [fi_mm]	Notch [mm]	CS [mm2]	Precrack [mm]	H [mm]
48	8	60	57.6	12	21.6	307.2	1	3

Prior to the test start the precracking procedure was carried out for each specimen, which goal was to create an initial crack of identical length (approximately 3 mm) for each specimen. The overall crack length throughout the test was derived using the susceptibility method [13]. This approach necessitates to monitor several

test parameters in order to derive the actual crack length using the equation provided in the standard [13]:

- W – characteristic dimension of each CT sample measured from the pin holes center to the rear of the sample,
- B – thickness of each specimen,
- E – Young's modulus – defined during the precracking stage,
- P – load force applied by the machine,
- u – crack displacement measured with a COD gauge (Fig. 4.3).

Each test was carried out using a different load sequence until the defined test limits were achieved, which were defined as the maximum displacement of the machine piston under the current load. The maximum load in each load sequence was around 4kN and it appeared several times throughout one sequence pass. Whenever this load caused the piston displacement to exceed the set value, the test halted and the specimen was considered fractured.

Figure 4.3. Test specimen placed in the test stand. During (with a COD gauge) and after the test

Additionally to the crack length definition method defined in the standard [13] an additional approach based on surface deformation measurements (Digital Image

Correlation) was used during the test. Therefore surface of each sample was covered in a special pattern. Correlation of crack length defined using the method described in the standard and the DIC method is beyond scope of this paper.

Test results and discussion

Crack propagation tests for the four defined load spectra were carried out and the obtained results are presented in Figure 4.4. The initial test using the load sequence based solely on the *SLMX14* strain gauge values resulted in 22.13 mm crack after 12 079 SFH. The test using load sequence based only on the nz load factor halted after reaching crack length of 28.50 mm after completion of 21 348 SFH, which is almost double the fatigue life of the comparative sequence. The *nz+Hb* sequence sample reached 26.07 mm in 17 664 SFH whereas the most complex *nz+Hb+Vp* sequence was the closest one to the comparative *SLMX14* sequence with 27.38 mm crack length and 13 401 SFH.

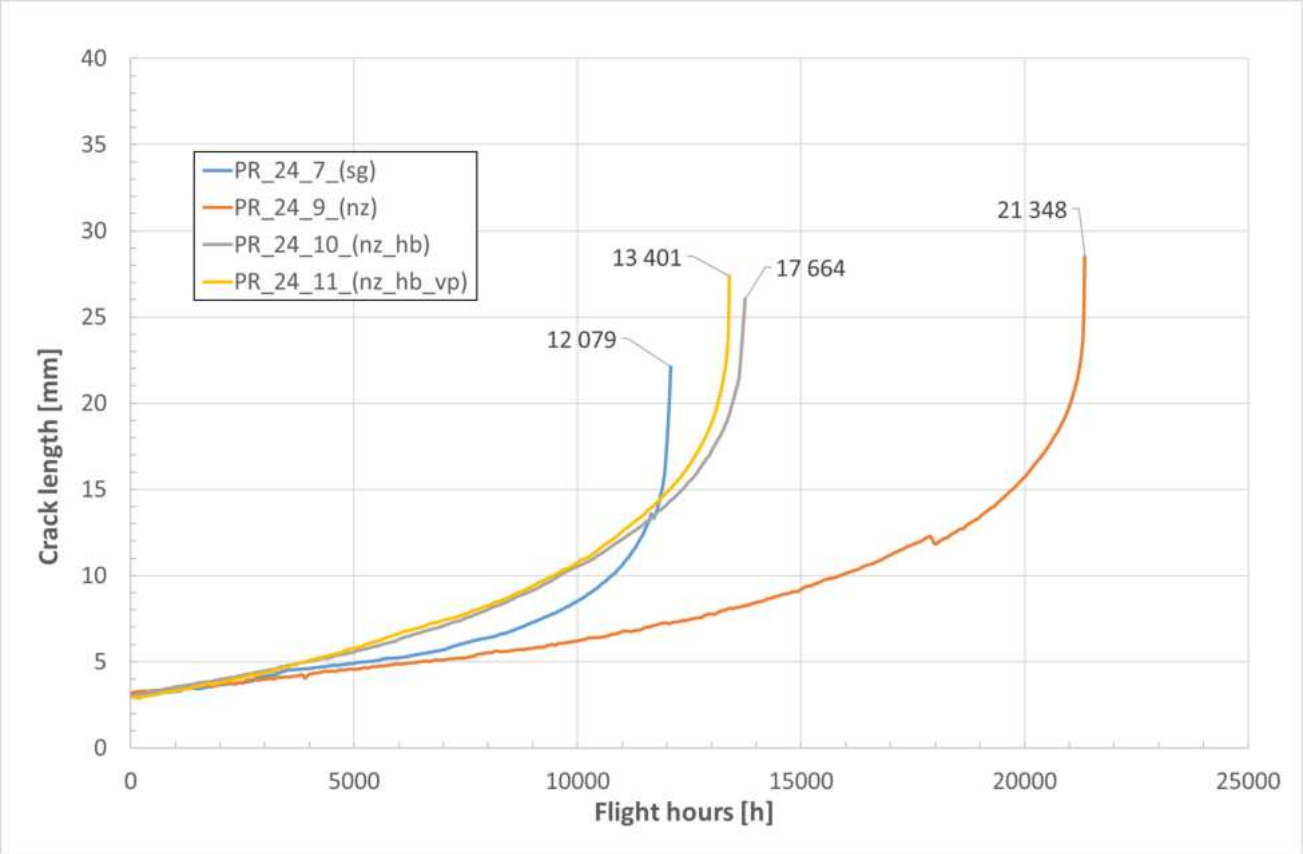

Figure 4.4. Crack propagation curves obtained for different load spectra

Preliminary results show, that using more detailed model incorporating more flight parameters, which show higher correlation with the main driving parameter, resulted in crack propagation estimation more similar to the one obtained with the comparative *SLMX14* load sequence. Small improvement in terms of a single load

value definition tends to result in higher fidelity in terms of additive crack propagation phenomena.

When direct load measurement is not financially justified using properly defined models based on the available data ma result in more reliable crack propagation estimations. Although the load factor is the main driver for wing loading it may be beneficial to incorporate more available flight data.

Further research will focus data loss mitigation, due to data mishandling and malfunction of the recording devices. Moreover the omitted control surface data could be taken into account, when specific flight mechanics formula will be used to make these data The missing data can be replaced using different techniques like linear regression models based on other available parameters or machine learning techniques.

Literature

1. Leski, A., Kurdelski, M., Reymer, P., Dragan, K., Sałaciński, M., Fatigue Life Assessment of PZL-130 Orlik Structure – Final Analysis and Results, Preceeding of the 28th ICAF Symposium, Helsinki, 5-5 June 2015
2. Reymer, P., Kurdelski, M., Leski, A., Leśniczak, A., Dziendzikowski, M., Introduction of an Individual Aircraft Tracking program for the polish Su-22, Fatigue of Aircraft Structures (2017), pp 101-108, DOI: 10.1515/FAS-2017-0008
3. MIL STD-1530D. Department of Defense Standard Practice Aircraft Structural Integrity Program (ASIP) 2016, US DoD
4. Jiao, R.; He, X.; Li, Y. Individual Aircraft Life Monitoring: An Engineering Approach for Fatigue Damage Evaluation. Chinese Journal of Aeronautics 2018, 31, doi:10.1016/j.cja.2018.02.002
5. Reymer, P.; Leski, A.; Kurdelski, M. Introduction of a Structure Integrity Program for a Military Trainer Aircraft. In Proceedings of the 28th Congress of the International Council of the Aeronautical Sciences 2012, ICAS 2012; 2012; Vol. 6
6. Gillet, O.; Bayart, B. Fatigue Crack Growth Approach for Fleet Monitoring. In Proceedings of the Lecture Notes in Mechanical Engineering; 2020A
7. Nesterenko, B.G.; Nesterenko, G.I.; Konovalov, V. v.; Senik, V.Y. Russian Practice to Provide Safe Operation of Airplane Structures with Long-Term Operation. In Proceedings of the Lecture Notes in Mechanical Engineering; 2020A

8. Molent, L.; Barter, S.A.; White, P.; Dixon, B. Damage Tolerance Demonstration Testing for the Australian F/A-18. International Journal of Fatigue 2009, 31, doi:10.1016/j.ijfatigue.2008.05.009
9. Daverschot, D.; Mattheij, P.; Renner, M.; Ardianto, Y.; de Araujo, M.; Graham, K. Full-Scale Fatigue Testing from a Structural Analysis Perspective. In Proceedings of the Lecture Notes in Mechanical Engineering; 2020Reymer, P., Leski, A., Flight loads acquisition for PZL-130 Orlik TCII Full Scale Fatigue Test, Fatigue of Aircraft Structures, Vol.1 (2011), pp 78-85
10. Kottkamp, E., Wilhelm, H., Kohl, D., NATO Advisory Group for Aerospace Research and Development, AGARDograph No. 160 Vol.7, April 1976
11. Jenkins, J. M., DeAngelis, V. M., A summary of numerous strain-gage load calibrations on aircraft wings and tails in a technology format, Nasa Technical memorandum 4804, Edwards, California 1997
12. Skopionski, T.H., Aiken Jr., W. S., Huston, W. B., Calibration of strain-gage installations in aircraft structures for the measurement of flight loads, NACA report nr 1178
13. ASTM E647-24, Standard Test Method for Measurement of Fatigue Crack Growth Rates. ASTM International, 2024

Contact: Piotr Reymer - piotr.Reymer@itwl.pl

5. I-31P Nose Landing Gear Dynamic Tests

(Zbigniew Skorupka - Łukasiewicz Research Network – Institute of Aviation, Warsaw, Poland)

The I-31 aircraft ((Fig. 5.1. - left) is redesigned version of the I-23 airplane ((Fig. 5.1. -right) - no major changes to design of its landing gears were made. There were changes made to some of the materials and manufacturing technologies.

Figure 5.1. I-31P (left) and I-23 (right) airplane. *Source:* L-ILot.

Nose landing gear

I-31P nose landing gear is a telescopic type landing gear equipped with oleo-gas shock absorber (Kowalski, W., et al., (2005), State of the art in landing gear shock absorbers. Transactions of the Institute of Aviation, 181(2), pp. 1-65). It is fully controllable/steerable by the pilot while on the ground and is equipped with wheel centering mechanism during retraction. Due to the mass and space restraints instead of full-fork for wheel support half-fork was used what resulted in much more stress prone design than full-fork.

Rest of the nose landing gear is quite typical aluminum/high strength steel design. In the Table 5.1. there are selected parameters of the nose landing gear and I-31P aircraft itself.

Table 5.1. I-31 Nose Landing Gear parameters

Parameter Name	Value	Unit
Configuration	telescopic	-
Aircraft Landing Mass	1117	kg
Aircraft Landing Weight	1096	daN
Vertical Landing Speed (Limit)	2,93	m/s
Horizontal Landing Speed (Limit)	37,8	m/s
Acceleration Coefficient during landing with Limit Vertical Landing Speed	4,86	-
Maximum Tyre Deflection	68	mm
Maximum Shock Absorber Deflection	124,6	mm

Description of the test procedure

- Tests were made according part 23 (CS, FAR) regulations to be compliant with existing certification (Normal, Utility, Aerobatic and Commuter Aeroplanes, CS-23, European Aviation Safety Agency (EASA), easa.europa.eu).
- Tests were made for two fillings/chargings of Shock Absorber. Technique and filling/charging parameters were the same. Differences in obtained results should be treated as envelope of landing gear parameters.
- There were suspicions that half-fork can be subjected to the excessive stress above material strength what can result in premature fatigue failure of the component. Strain gauges were applied (Fig. 5.2 - 5.3) in order to collect data that correspond to the obtained loads and landing cases.
- As reference and as input parameters for performing drop test the parameters from certification tests of I-23 Nose Landing Gear were taken (Tab. 5.2.).

Table 5.2. Input Parameters and reference values of the tests

Input Parameters		
Parameter Name	Value	Unit
Shock Absorber Pressure	0,95	MPa
Tyre Pressure	0,31	MPa
Vertical Landing Speed (Limit)	2,93	m/s
Horizontal Landing Speed (Limit)	37,8	m/s
Reference Values		
Vertical Force (Fz)	17,38	kN
Horizontal Force (Fx)	6,40	kN
Acceleration Coefficient (nz)	4,86	-
Landing Gear Deflection (Uk)	183,5	mm
Shock Absorber Deflection (Ua)	115,8	mm

Figure 5.2. Strain gauge placement on NLG half-fork. *Source:* L-ILot.

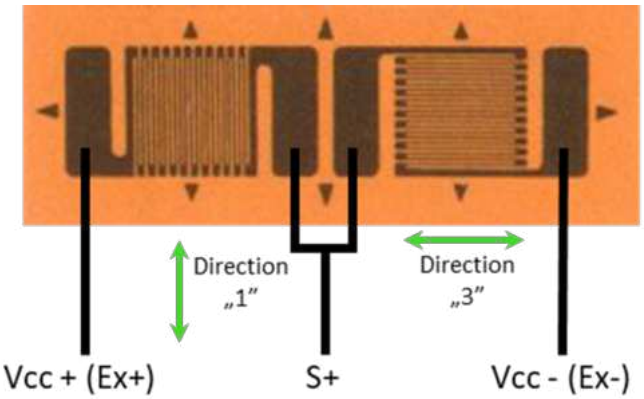

Figure 5.3. Strain gauge configuration. *Source:* L-ILot.

Strain gauges used: Tenmex TFxy-4/120, k=2,19±0,5%, R=120,2[Ω]±0,2%, direction ”1” – along half-fork axis, Direction”3” - across half-fork axis

Measurement points:

- ZD – outside (opposite to wheel axis side) bottom.
- WD – outside (opposite to wheel axis side) bottom.
- ZG – inside (wheel axis side) top.
- WG – inside (wheel axis side) top.

Static tests

Static tests of the shock absorber were made according to the Technical Specification (WT-800.42.10, Warunki Techniczne Samolotu I-23, Amortyzator Podwozia przedniego, Nr. rys. 800.42.10.00) of the I-23 aircraft. Static characteristic was made using the 40/20T Press test stand (Fig. 5.4) in Landing Structures Testing Laboratory (former Landing Gear Laboratory) in Lukasiewicz Research Network – Institute of Aviation. The tests stand is a hydraulic press designed to be able to act as high load strength machine for shock absorber and wheel testing.

Test stand parameters:

- Forces: Vertical up to 392kN, Horizontal force up to 196kN
- Total vertical displacement 400mm
- Velocities: Vertical up to 300mm/min, Horizontal up to 600mm/min
- Work area: Horizontal 800 x 760mm, Vertical 190 up to 2000mm
- Force or displacement control (continuous or step)
- Force and displacement acquisition (and up to 8 external analogue signals)

Scope of tests: static tests, force-displacement characteristics, shock absorbers, dampers, material characteristics, wheel static tests.

Two sets of static characteristics were made in order to achieve the load envelope for the shock absorber parameters. Thow separate filings/chagrins of the shock absorber were made using the concept to use the same parameters and techniques for every shock absorber filling/charging. Static tests were also separated by the dynamic tests for each filling/charging.

Figure 5.4. 40/20T Press. *Source*: Landing Gear Laboratory, L-ILot.

Example of results from static tests of I-31P nose landing gear are shown in Fig. 5.5 and 5.6:

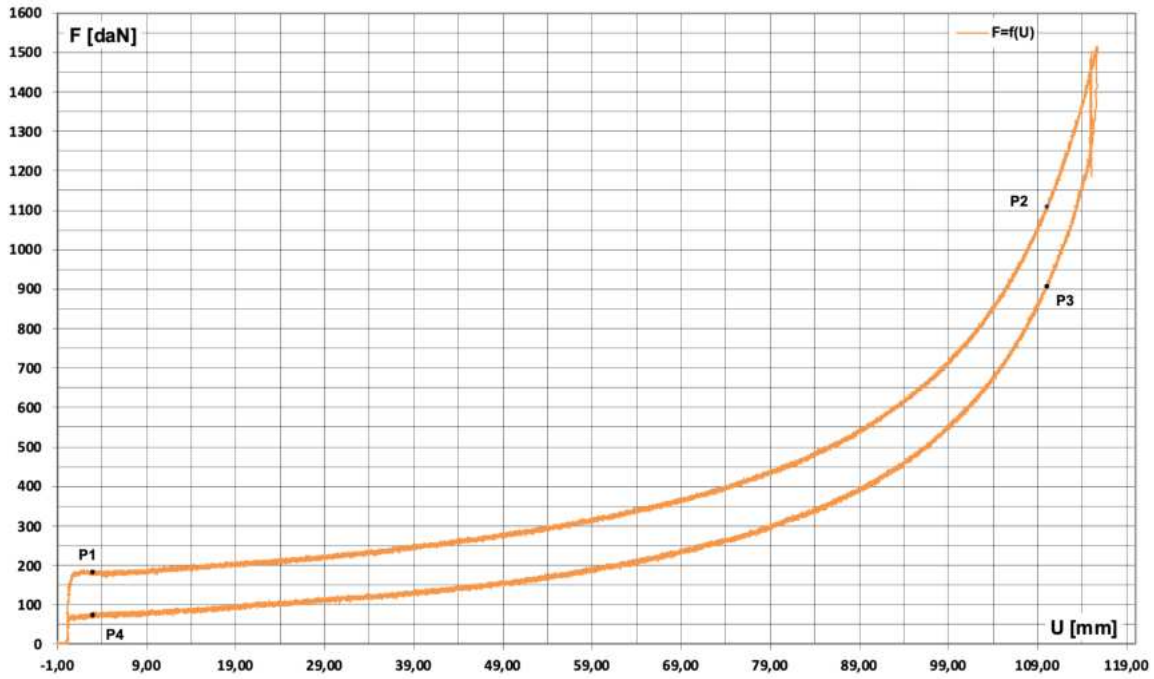

Figure 5.5. 1st filling/charging, 0326-I31PP-st-P40-0031. *Source*: L-ILot.

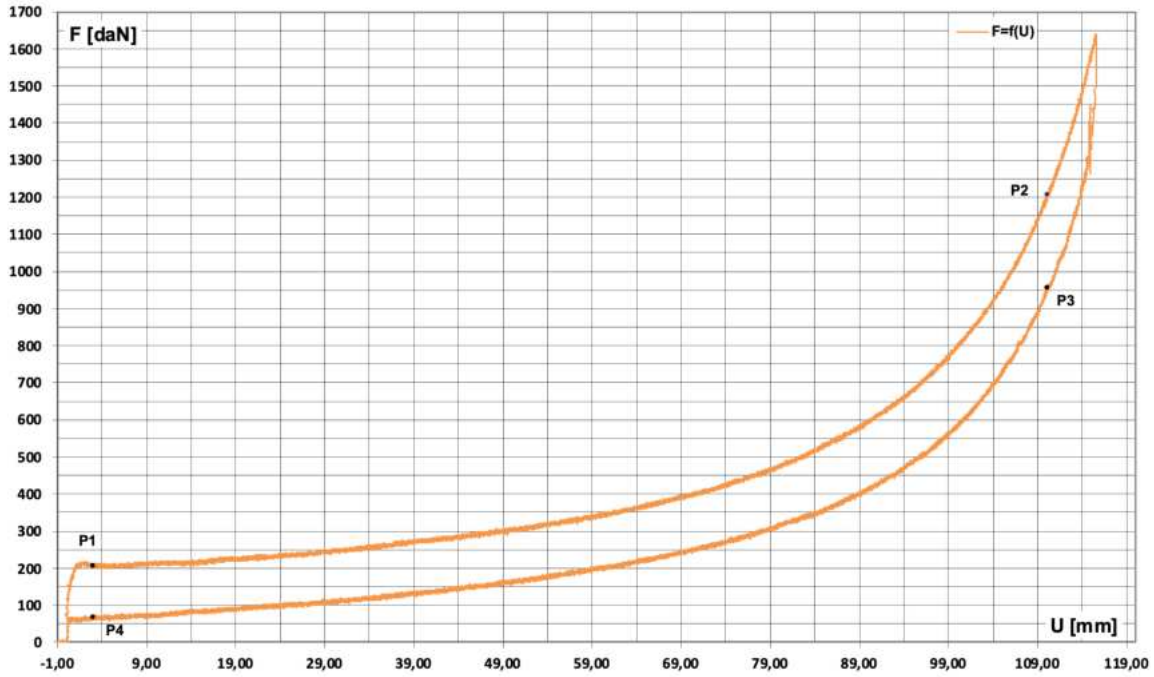

Figure 5.6. 2nd filling/charging, 0326-I31PP-st-P40. *Source*: L-ILot.

Dynamic tests

Dynamic tests of the landing gears are simply the simulations of the landing itself in controlled environment. In order to achieve the correct effect drop test stands (other name: drop test hammers) are used. These test stand are built in order to be support for the landing gear with the test enabling hardware and not to interfere (introduce friction which can reduce energy dissipated by the landing gear and undesirable lower the loads acting on the fuselage) with the process which is free drop from the height corresponding the desired landing speed (Skorupka, Z., Laboratory Investigations on Landing Gear Ground Reactions (Load) Measurement, Journal of KONES Vol. 24/ No. 2, 2017, p. 225-230, ISSN 1231-4005, eISSN 2354-0133). The parameters of the drop tests were taken from the certification tests of the I-23 nose landing gear as reference (Tab. 5.2. and 14/ZB/BW-C6/00, Zeszyt Badań, Podwozie Przednie s-tu I-23, 11.2000). Landing gear was prepared according to the Techical Specification of I-23 (WT-800.42.00, Warunki Techniczne Samolotu I-23, Podwozie przednie, nr rys. 800.42.00.00.00) and technical documentation of I-31P nose landing gear (3900.042.100.000.00, Podwozie przednie).

Test were performed on M10T (Fig. 5.7) drop test stand in Landing Structures Testing Laboratory (former Landing Gear Laboratory) in Lukasiewicz Research Network – Institute of Aviation.

Below there are M10T test stand parameters:

- Maximum mass of test object including mounting parts: 10T
- Maximum forces in drop tests: Vertical: 392kN, Horizontal: 196kN, Side: 157kN
- Maximum buffer pressure (lift): 3 MPa
- Maximum wheel spin up velocity: 111 m/s
- Maximum free fall velocity up to 8 m/s – varies on test object height

Scope of tests: drop tests, wheel static tests, and functional tests.

As in the case of static tests, drop tests were performed in two sets for different fillings/chargings. Test results are presented in the Figures 5.8 to 5.11.

Figure 5.7. M10T test stand – overview example (left), I-31 NLG mounted (right). *Source*: L-ILot.

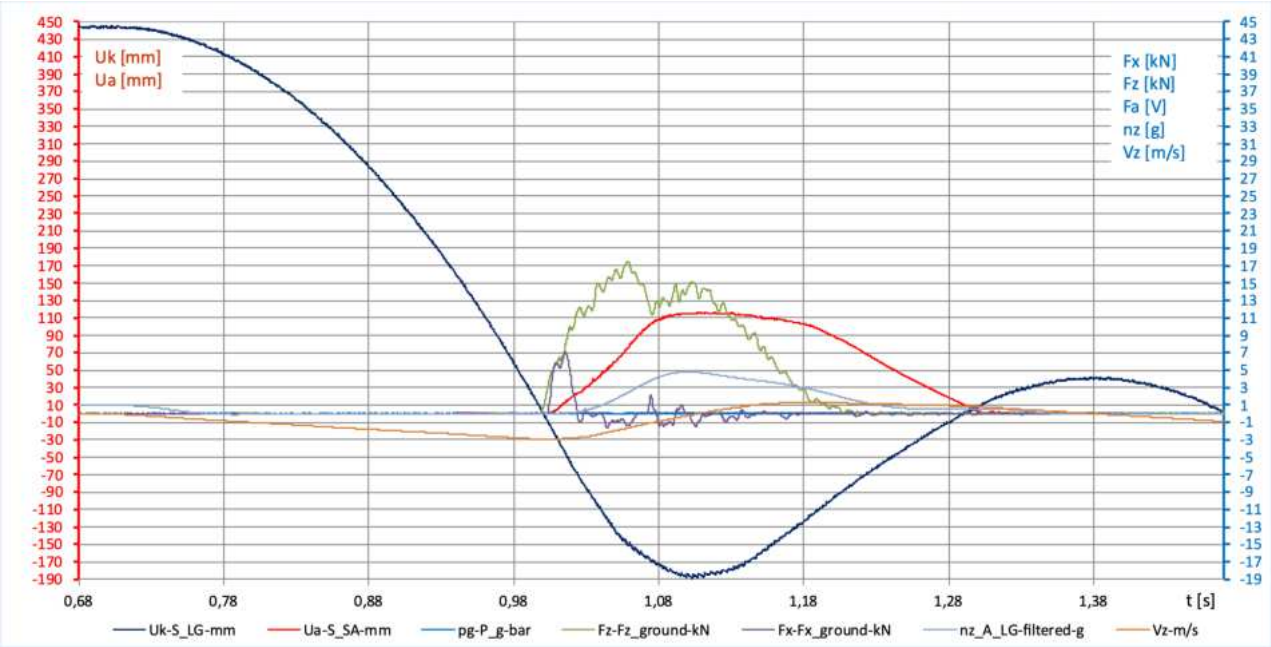

Figure 5.8. Example of full-scale dynamic I-31 NLG drop tests, general results. 1st filling/charging, 0326-dt-NLGI31-M10T-064. *Source*: L-ILot

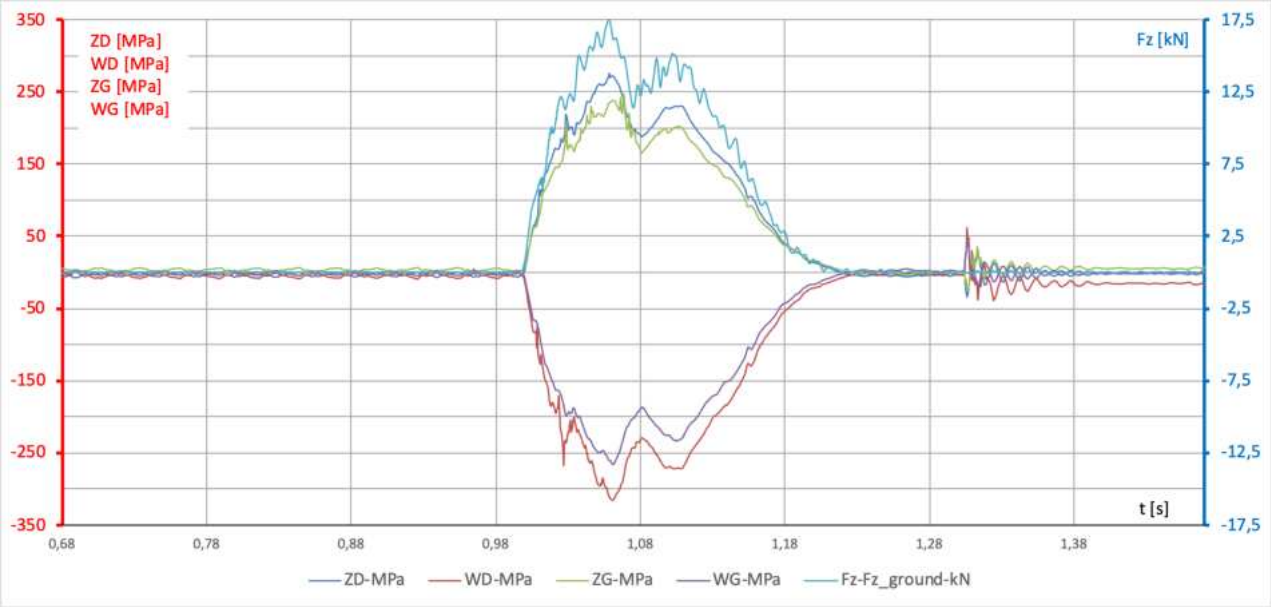

Figure 5.9. Example of full-scale dynamic I-31P NLG drop tests, strain gauge results. 1st filling/charging, 0326-dt-NLGI31-M10T-064. *Source*: L-ILot

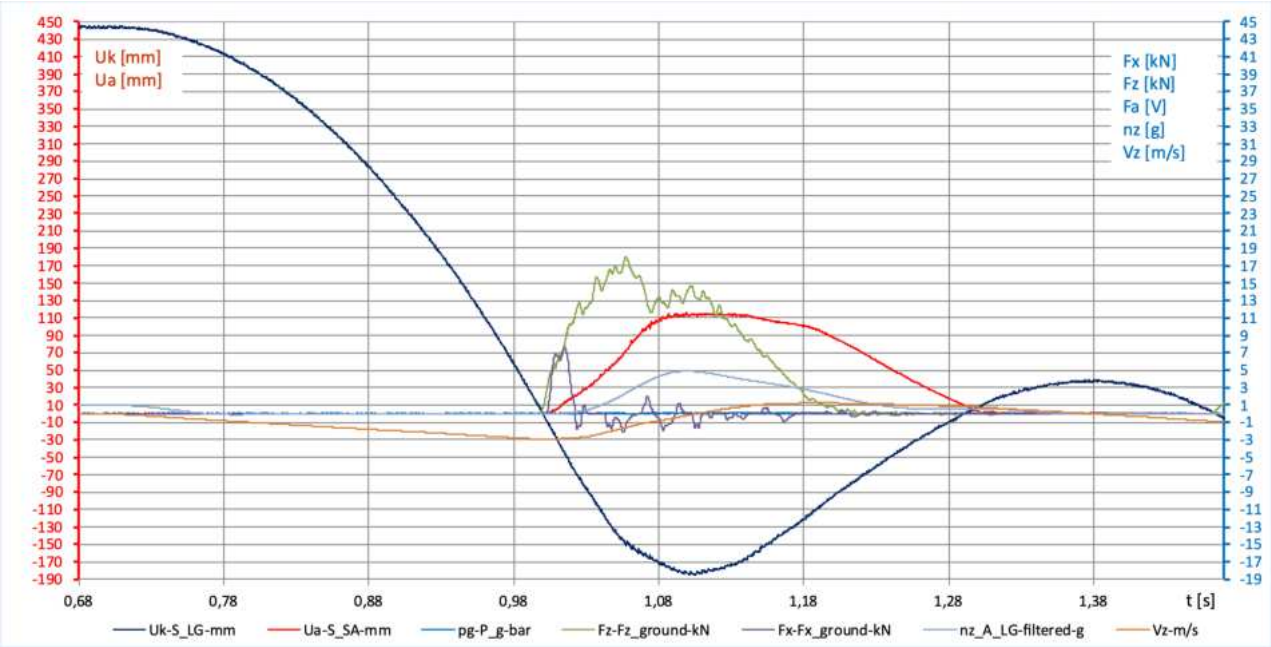

Figure 5.10. Example of full-scale dynamic I-31P NLG drop tests, general results. 2nd filling/charging, 0326-dt-NLGI31-M10T-094. *Source*: L-ILot

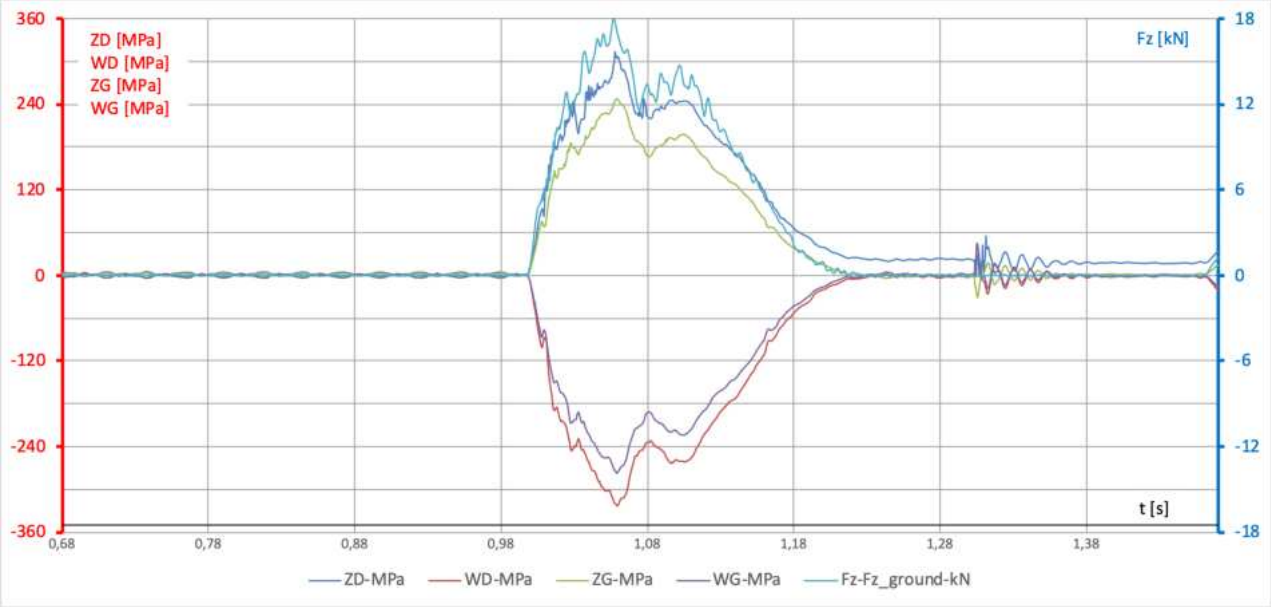

Figure 5.11. Example of full-scale dynamic I-31P NLG drop tests, strain gauge results. 2nd filling/charging, 0326-dt-NLGI31-M10T-094. *Source*: L-ILot

5. Test results - comparison

The results obtained in all test categories are summarized below in the Tables 5.3 to 5.5.

Table 5.3. Dynamic Tests (Limit Conditions)

Parameters	Reference	1 s t charging	2nd charging	
Parameter Name	Value			Unit
Shock Absorber Pressure	0,95			MPa
Tyre Pressure	0,31			MPa
Landing angle (φ)	0°			
Vertical Landing Speed (Vz)	2,93	2,93	2,93	m/s
Horizontal Landing Speed (Vx)	37,8	39,06	40,07	m/s
Vertical Force (Fz)	17,38	17,47	18,04	kN
Horizontal Force (Fx)	6,40	7,1	7,6	kN
Acceleration Coefficient (nz)	4,86	4,80	4,89	-
Landing Gear Deflection (Uk)	183,5	189,3	185,8	mm
Shock Absorber Deflection (Ua)	115,8	116,1	114,3	mm

Table 5.4. Dynamic Tests (Limit Conditions) – Strain on Half Fork

Parameters	1 s t charging	2nd charging	
	Value		Unit
ZD - outside (opposite to wheel axis side) bottom	275,67	313,52	MPa
WD -outside (opposite to wheel axis side) bottom	-316,13	-323,31	MPa
ZG - inside (wheel axis side) top	246,59	248,41	MPa
WG - inside (wheel axis side) top	-266,32	-277,75	MPa
Vertical Force (Fz)	17,47	18,04	kN

Table 5.5. Static Tests/Characteristics

Characteristic points	1st charging	2nd charging	
	Value		Unit
P1	182	207	daN
P2	1109	1206	daN
P3	904	956	daN
P4	74	68	daN

7. Summary

- Change of manufacturer or/and updates of materials and technologies in landing gears results in need for repeating the certification tests.
- As reference for the tests results from previous certification tests were used.
- Due to suspicions about the strength of half-fork the strain gauges were applied in designates areas.
- Tests proven the landing gear operation and replicated the previous results with acceptable repeatability.
- Tests were made for two fillings/chargings of Shock Absorber. Technique and filling/charging parameters were the same. Differences in obtained results should be treated as envelope of landing gear parameters.

References

- Currey, N.S., Aircraft Landing Gear Design Principles and Practices, Washington AIAA 1988.10.2514/4.861468
- Reymer P., Leski A., Zielinski W., Jankowski K., Full Scale Fatigue Test concept of a Su-22 fighter bomber, Fatigue of Aircraft Structures 6, 79-87
- Leski A., Reymer P., Kurdelski M., Development of load spectrum for full scale fatigue test of a trainer aircraft, ICAF 2011
- Kowalski, W., et al., (2005), State of the art in landing gear shock absorbers. Transactions of the Institute of Aviation, 181(2), pp. 1-65
- Kurdelski M., Leski A., Crack Growth Analysis of the Landing Gear Pull Rod of the Fighter Jet Aircraft, Fatigue of Aircraft Structures, 2011 (3), 64-73
- Dziendzikowski M., Kurnyta A., Reymer P., Kurdelski M., Klysz S., Leski A., et. al., Application of operational load monitoring system for fatigue estimation of main landing gear attachment frame of an aircraft, Materials 14 (21), 6564

- Skorupka Z., Tywoniuk A., Health Monitoring in Landing Gears, Journal of Kones, 2019, 1(26), 167-174
- Normal, Utility, Aerobatic and Commuter Aeroplanes, CS-23, European Aviation Safety Agency (EASA), easa.europa.eu
- WT-800.42.10, Warunki Techniczne Samolotu I-23, Amortyzator Podwozia przedniego, Nr. rys. 800.42.10.00
- Skorupka, Z., Laboratory Investigations on Landing Gear Ground Reactions (Load) Measurement, Journal of KONES Vol. 24/ No. 2, 2017, p. 225-230, ISSN 1231-4005, eISSN 2354-0133
- 14/ZB/BW-C6/00, Zeszyt Badań, Podwozie Przednie s-tu I-23, 11.2000
- WT-800.42.00, Warunki Techniczne Samolotu I-23, Podwozie przednie, nr rys. 800.42.00.00.00
- 3900.042.100.000.00, Podwozie przednie

Contact: Zbigniew Skorupka - Zbigniew.Skorupka@ilot.lukasiewicz.gov.pl

6. NDT Robotic System for Bonded Repair Diagnostic - Design and Evaluation

(Michał Siniarski, Piotr Synaszko, Krzysztof Dragan - Air Force Institute of Technology, Warsaw, Poland)

Aircraft require periodic inspections in accordance with procedures developed by manufacturers and approved by the competent aviation authorities. During inspections, damages caused by fatigue, corrosion or incidents are detected. In most cases, these damages are repaired according to procedures. In many cases, composite repairs are used. According to recommendations [1] some NDT methods are used to confirm quality of the repair. Most common used way to perform NDT inspection is manual A-scan. Manual testing results in many inconsistencies such as uneven angle and value of pressing force of the probe. These matters may lead to unrepeatable, less reliable results. Automation of the tests offers an improvement in their precision and increase in speed [5, 6]. It also gives more informative data and allows to reduce costs by minimizing the service time. There are many different approaches to automation systems. They vary in the operation concepts and their use cases. Most common [7, 5, 8] are:

- Robot driving on examined surface
- Robot arm,
- Probe shifting along two axes (XY scanner).

Each system gains some advantages over the others when operating in certain. Despite their high reliability and speed, nowadays automated systems tend to be expensive, complex solutions with very few features extensions possibilities.

This work's aim was to simplify above problem by designing an automated NDT system, and evaluate its performance in terms of testing results reliability and quality of using the system. Desired outcome can be achieved by combining features and characteristics of commercial tools and technical solutions necessary for workflow and architecture simplicity.

Above matters lead to conclusions about main needs designed system has to fulfill. Designed system aims to be primarily:

- Creating reliable, readable results,
- Simple and low cost in construction,
- Made of parts generally available on the market,
- Open software, enabling user to expand its functionality, use different testing methods,
- Simple and intuitive to use.

The project in the test phase utilizes two NDT methods, which are:

- Mechanical Impedance Analysis (MIA):

  The method used to detect delaminations in composites, metals and bonded structures [9] is based on measurements of harmonic force probe input to the point of a surface and resultant velocity of this point [10]. Above values result with impedance [9, 10]

$$Z = \frac{F}{\nu}$$

  The method is sensitive to surface stiffness, thickness, elastic properties and density changes [9, 10]. As long as all layers are bonded the received signal keeps high values and hence it drops once the flaw is detected [9].

- Eddy Current Testing (ET):

  Method finds use in inspecting metal structures for both surface and subsurface defects [11]. It functions on the basis of electromagnetic induction [12]. Field causes eddy current flow in the test sample, which creates its own electromagnetic

field, weakening the original one. Above dependence allows to detect cracks by impedance signal change [11].

It is worth noting that both described methods are comparative. It means it is necessary for proper results evaluation to compare them with the ones obtained for standardized sample with known and accurate characteristics.

System Configuration

In order to fulfill the needs stated in the previous chapter specific parts were chosen. System's main concept is based on robotic arm (Dobot Magician) operating in cartesian coordinate system. Arm has 3 degrees of freedom which leads to poor geometry irregularities reduction. To improve this probe spring suspension is used. Probe signal is sent in real-time to flaw detector which translates it to voltage signal and transits it into Raspberry Pi 4B computer. All the hardware is managed by the Python software developed by authors. To ensure the ease of use of the system control program is equipped with Graphical User Interface which guides user through the scanning process, enabling him to choose proper working parameters (such as resolution, sample size, plot type). It also postprocesses acquired data and plots it desired way. Relation between main components of system are shown on Figure 6.1.

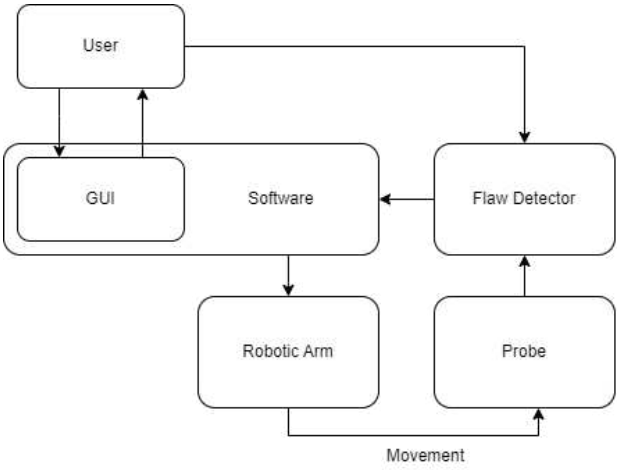

Figure 6.1 System diagram

Figure 6.2 System assembly

As a result the system is an open loop one with no possibility of arm movement inaccuracies reduction. It is not seen as an issue due to the decent robot precision, although it is also an area for future closed loop systems applications. Such configuration maintains high modularity which enables the user to replace scanner parts or extend its functionality. As a flaw detectors OLYMPUS family flaw detectors

(NORTEC, BondMaster) were used. Equipped with standardized VGA conectors they made possible to acquire measurement signals. Regardless of the defectoscope, the captured signal is within a similar voltage range, which makes it easy to change the application of the system.

Testing Results

Tests of two samples were conducted. First of them required MIA method. Standardized sandwich sample was made of glass and carbon fibre skins and nomex honeycomb core

- Such kind of structures are widely used in the aerospace industry since they are a combination of high stiffness and low mass [13].

Figure 6.3. Sample 1. (used for MIA testing)

Collected data is visualized as C-scans. Plots are elaborated in different colors, in 2D, which is usually more legible and 3D which happens to be more informative in some specific use cases.

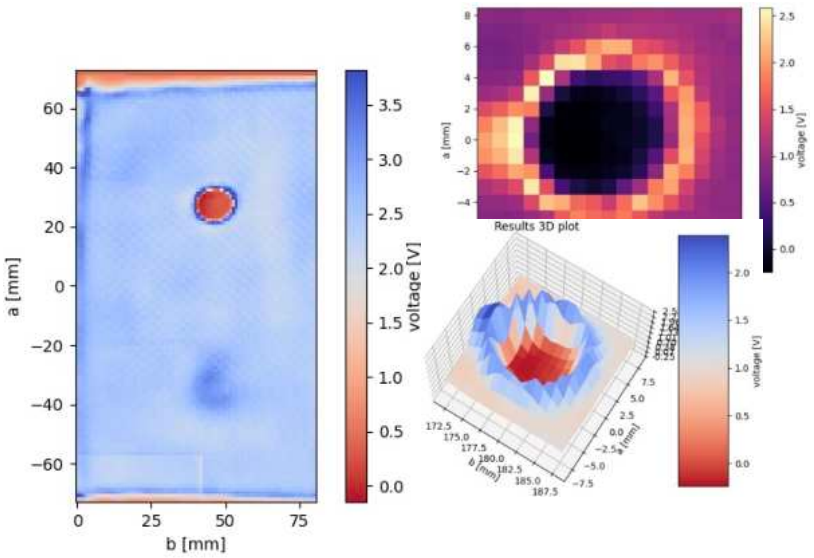

Figure 6.4. MIA results for sample 1.

Second sample is aluminum plate with repair patch above simulated cracks with different lengths. Another feature differing this element from previous one is its curvature which may cause complications during scanning and printing results on flat surface.

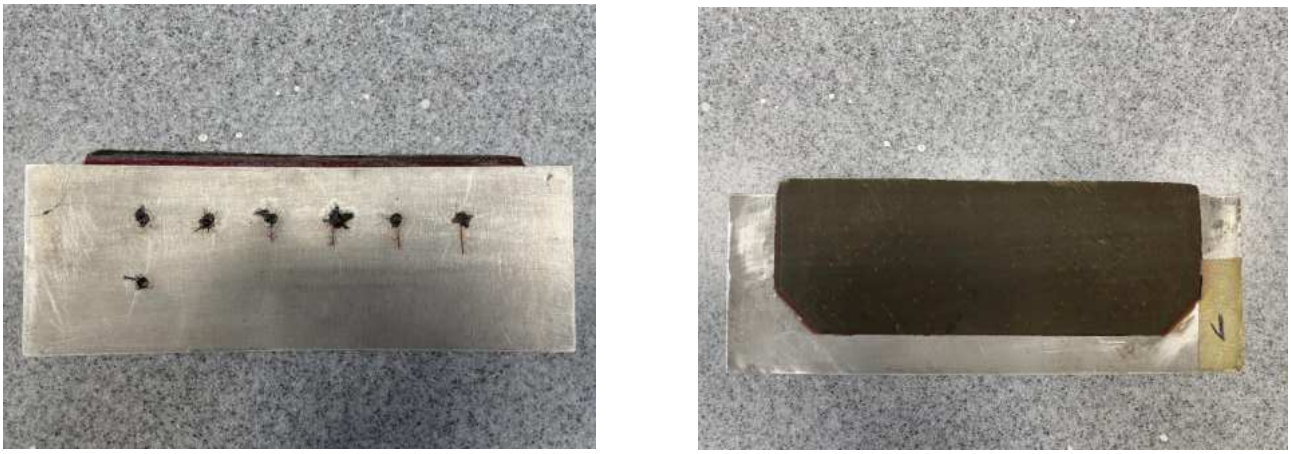

Figure 6.5. Sample 2. for ET testing method

Element requires ET method for testing. Results are drawn the same way as before:

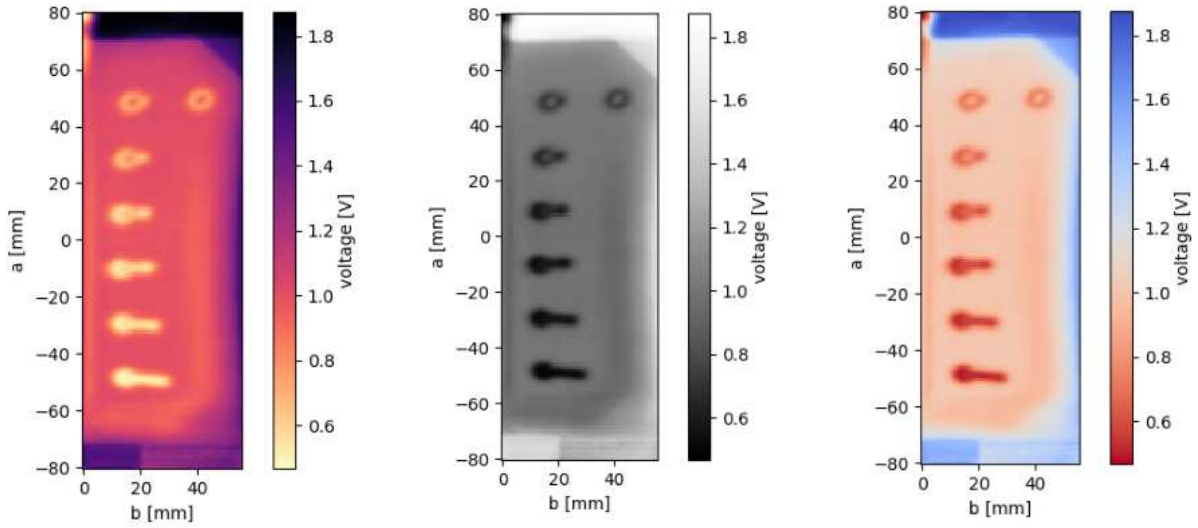

Figure 6.6. ET results for sample

System Evaluation

For quantitative evaluation numerical comparisons of results acquired by designed tool and commercial tool (MAUS V) were made. The scaling objects of analysis for each sample was sample 1.: tested with MIA method. For both systems resultant image was scaled first due to the known size of the label sticker placed on the outer surface, which made it possible to measure carbon-fiber disbond. Such comparison is considered as reliable since sticker's size is manually measurable. Both plots are shown on Figure 6.7 a) and b).

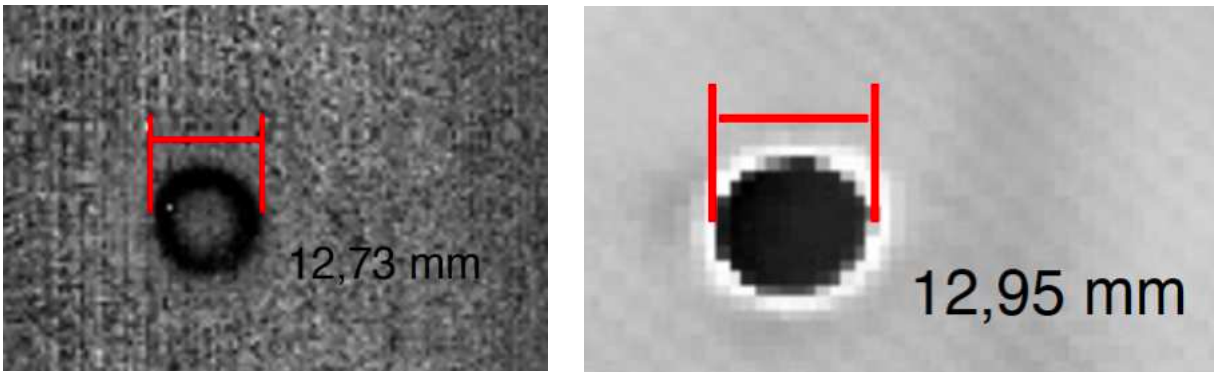

Figure 6.7 a) results obtained with MAUS V system b) results obtained with designed system

The dimension deviation is acceptably low which proves design test system reliability. Analogous analysis wasn't conducted for sample 2., but visible distortion indicates the presence of higher dimensions deviation for both systems.

Qualitative evaluation is based on the presented results, workflow experience and final compliance with assumptions stated in the INTRODUCTION section. All the defects on both samples are visible, hence possible to detect. Plots are clear and look similar to ones achievable with commercial scanners. Shape for sample 1. is well preserved, however there is an image distortion for sample 2. This issue doesn't affect plot readability. Tool is built with market accessible parts, which cost is relatively low. The total cost of all the parts used is about 40 times lower than price of the MAUS V system.

<table>
<tr><td colspan="2">MAUS V</td><td colspan="2">DESIGNED SYSTEM</td></tr>
<tr><td>ELEMENT</td><td>PRICE</td><td>ELEMENT</td><td>ESTIMATE PRICE</td></tr>
<tr><td rowspan="5">Whole system</td><td rowspan="5">500 000 USD</td><td>Robotic arm</td><td>2 000 USD</td></tr>
<tr><td>Composite Bond Tester</td><td>10 000 USD</td></tr>
<tr><td>Raspberry Pi 4B and accessories</td><td>200 USD</td></tr>
<tr><td colspan="2">TOTAL</td></tr>
<tr><td colspan="2">12200 USD</td></tr>
</table>

Table 6.1. Approximate cost of both compared systems

Each part is connected in an uncomplicated way – connections are made with widely available interfaces (like USB, or ones standardized for NDT testers). Field of workflow facilities and improvements are provided by software and built-in GUI.

Problems the scanner faces is low scanning speed. The issue is caused by programming language choice: Python despite being simple and proper tool for prototyping new functions forces arm to operate only one step at a time.

Conclusions

Designed system complies with assumptions stated in the INTRODUCTION paragraph. System is modular, easy to use and the time to start an examination is relatively short. Obtained results are reliable and for most cases accurate. Above achievements in combination with low cost make the system an attractive solution for testing automation with possibilities to customize it to personal preferences.

Problems the system faces are mostly scanning speed, limited range of movement and results distortion for more complex geometries. As presented system is highly modular, most of this issues can be resolved with module replacement or software improvement. Such further steps are planned for future development.

Bibliography

[1] SAE International Recommended Practice, COMPOSITE REPAIR NDT/NDI HANDBOOK, SAE Standard ARP5089, Reaffirmed November 2011, Issued November 1996, https://doi.org/10.4271/ARP5089

[2] P. Zientek, "Metody badań nieniszczących wybranych elementów konstrukcji turbozespołu małej mocy," *Maszyny Elektryczne: zeszyty problemowe,* vol. 3, p. 115–120, 2016.

[3] K. Onoszko, "Metody stosowane w badaniach nieniszczących," *Informatyka, Automatyka, Pomiary w Gospodarce i Ochronie Srodowiska,* p. 11–14, 2012.

[4] B. Kamsu-Foguem, "Knowledge-based support in Non-Destructive Testing for health monitoring of aircraft structures," *Advanced Engineering Informatics,* vol. 26, pp. 859-869, 2012.

[5] M. Morozov, S. G. Pierce, C. N. MacLeod, C. Mineo and R. Summan, "Off-line scan path planning for robotic NDT," *Measurement,* vol. 122, pp. 284-290, 2018.

[6] V. GOVINDARAJU and G. PALANISAMY, "Need of robotic systems in non-destructive testing applications," in *ND E 2017 Conf. & Exhibition of the Indian Soc. for NDT (ISNT)*, 2017.

[7] "Aviation Week: Invert Robotics Adding NDT Tech To Mobile Climbing Robots," 20019.

[8] J. Buckley, R. Smith and J. Skramstad, "TRANSIENT EDDY CURRENTS FOR AIRCRAFT STRUCTURE INSPECTION - AN INTRODUCTION," January 2003.

[9] Y. V. LANGE, "THE MECHANICAL IMPEDANCE ANALYSIS METHOD OF NONDESTRUCTIVE TESTING (A REVIEW)," *Nondestructive Testing and Evaluation,* vol. 11, pp. 177-193, 1994.

[10] P. Cawley, "The sensitivity of the mechanical impedance method of nondestructive testing," *NDT International,* vol. 20, pp. 209-215, 1987.

[11] J. García-Martín, J. Gómez-Gil and E. Vázquez-Sánchez, "Non-Destructive Techniques Based on Eddy Current Testing," *Sensors,* vol. 11, p. 2525–2565, 2011.

[12] A. Kondej, T. Babul and S. Joñczyk, "Aparatura i możliwosci badań nieniszczących metodą prądów wirowych w Instytucie Mechaniki Precyzyjnej," *Badania Nieniszczące i Diagnostyka,* vol. nr 3, p. 38–42, 2017.

[13] G. Wróbel, Ł. Wierzbicki, Ł. Siódmok and K. Nowakowski, "Wytrzymałość na ścinanie międzywarstwowe kompozytów przekładkowych," *Przetwórstwo Tworzyw,* vol. 21, p. 61–64, 2015.

[14] G. Wróbel and S. Pawlak, "A comparison study of the pulse-echo and through-transmission ultrasonics in glass/epoxy composites," *Journal of Achievements in Materials and Manufacturing Engineering,* vol. 22, June 2007.

Contact: Michał Siniarski - michał.siniarski@itwl.pl

7. Using Corrosion Health Monitoring Systems to Detect Corrosion: Real-Time Monitoring to Maintain the Integrity of the Structure

Patryk CIĘŻAK[1], Lourdes VAZQUEZ-GOMEZ[2], Luca MATTAROZZI[2], Alessandro BENEDETTI[2], Jakub KOTOWSKI[3], Piotr SYNASZKO[3], Krzysztof DRAGAN[3], Dominik GŁOWACKI[4], Konrad WAWRYN[5]

1) Military University of Technology (Poland)
2) National Research Council – Institute of Condensed Matter Chemistry and Technologies for Energy (Italy)
3) Air Force Institute of Technology (Poland)
4) Warsaw University of Technology (Poland)
5) UMF - Unique Model Factory (Poland)

Introduction

Atmospheric corrosion is a pervasive issue affecting various industries, with airports and the aviation sector being particularly vulnerable due to their exposure to harsh environmental conditions. This work overviews atmospheric corrosion and the factors influencing its occurrence, including the mechanisms behind it, the specific challenges faced by airports and aircraft producers, and the mitigation strategies employed to combat this persistent threat. The goal is to emphasize the importance of proactive corrosion management in ensuring the safety, reliability, and longevity of aviation assets.

Mechanisms of Atmospheric Corrosion

Atmospheric corrosion occurs through electrochemical reactions between metal surfaces and environmental elements. Key factors influencing these reactions include:

- Humidity and Moisture: The presence of water, whether in liquid form or as vapor, facilitates the electrochemical processes that lead to corrosion. High relative humidity levels can accelerate these reactions, while dew, rain, and fog contribute to the persistence of moisture on surfaces.
- Temperature: Elevated temperatures generally increase the rate of corrosion reactions. However, temperature fluctuations can also cause condensation, creating localized areas of high moisture concentration that promote corrosion.

- Pollutants: Industrial pollutants such as sulfur dioxide (SO_2) and nitrogen oxides (NO_x) react with moisture to form acidic compounds, which can significantly accelerate corrosion. Additionally, chlorides, especially in marine environments, are highly aggressive towards metals.
- Material Composition: Different metals and alloys exhibit varying levels of susceptibility to atmospheric corrosion. Protective coatings and treatments can enhance the resistance of these materials to corrosive processes.

Introduction to CHM Systems

Corrosion Health Monitoring (CHM) systems are advanced technologies and methodologies used to detect, monitor, and assess corrosion in structures and materials, particularly those exposed to harsh environments. These systems leverage various sensors, data acquisition tools, and analytical methods to provide real-time or periodic information about the condition of materials and structures.

Purpose of Corrosion Health Monitoring Systems

Early detection and prevention of corrosion are crucial. CHM systems detect the early stages of corrosion before it leads to significant material degradation. By catching corrosion early, CHM systems help in preventing sudden and catastrophic structural failures. Providing real-time data allows for timely maintenance, which can extend the life of assets.

With accurate corrosion data, maintenance can be performed only when necessary, reducing downtime and maintenance costs. Continuous monitoring ensures that the structural integrity of critical infrastructure is maintained, enhancing overall safety. CHM systems also help ensure compliance with industry safety standards and regulations. Early detection reduces the need for emergency repairs, which are often more costly. Maintenance resources can be better allocated based on actual corrosion data rather than estimated schedules.

CHM systems provide valuable data that can be used for making informed decisions regarding asset management and maintenance. Advanced CHM systems can use collected data for predictive analytics, helping forecast future corrosion trends and potential issues. By implementing CHM systems, industries can significantly enhance the safety, reliability, and longevity of their assets while reducing costs and environmental impact.

Impact on Aircraft and on Airport Infrastructure

Impact on Aircraft

Selecting optimal locations for sensor placement in the aircraft is an inherently complex and time-consuming task. Sensors need to be installed in areas where corrosion is anticipated to be most severe, ideally based on a comprehensive database detailing observed corrosion hotspots for the specific aircraft type. However, creating such a database requires long-term monitoring and the deployment of the system on already well-documented structures. For instance, the installation of the CHM system on the Mi-24 helicopter used by the Polish Armed Forces (Fig. 7.1) leverages existing knowledge of the helicopter's structural vulnerabilities, making it easier to strategically place sensors to effectively monitor and mitigate corrosion (Ciężak & Rdzanek, 2020).

Figure 7.1. CHM system consisting of three autonomic sensors installed on in-service Mi-24

Aircraft are constructed from a variety of materials, including aluminum alloys, steel, and composites, each with differing susceptibilities to corrosion, which have different effects on the fatigue behavior of the structure. Specific corrosion-prone areas include:

- Fuselage Corrosion: Aluminum alloys, commonly used in aircraft fuselages, are prone to pitting and intergranular corrosion, which can lead to structural weaknesses and increased drag, affecting the aircraft's performance and fuel efficiency.

- Wing and Tail Structures: These critical components are exposed to various environmental conditions and are at risk of corrosion, which can compromise their aerodynamic properties and structural integrity.

Corrosion poses severe safety risks to aircraft. Structural failures due to corrosion can lead to catastrophic incidents – such as that of Aloha Airlines Flight 243 (National Transportation Safety Board, 1988). Additionally, corrosion of electrical and hydraulic systems can cause malfunctions that impair the aircraft's operational capabilities. Therefore, rigorous inspection and maintenance protocols are essential to ensure flight safety.

To counteract the effects of atmospheric corrosion, aircraft maintenance involves regular inspections, repairs, and replacements. These activities increase operational cost and require significant resources. While using corrosion-resistant materials and advanced protective coatings can extend the service life of aircraft and improve safety, they also add to costs.

Effective mitigation of atmospheric corrosion involves a combination of material selection, protective measures, and proactive maintenance practices:

- Protective Coatings: Application of corrosion-resistant paints and coatings is a primary defense against atmospheric corrosion. Galvanization, which involves coating steel with a layer of zinc, is particularly effective for protecting steel structures.
- Material Selection: Utilizing alloys with high corrosion resistance and incorporating non-metallic composite materials can significantly reduce the susceptibility of components to corrosion.
- Environmental Control: Managing humidity levels and reducing exposure to corrosive pollutants are crucial steps in minimizing corrosion risks. This can involve the use of dehumidification systems and pollution control measures.
- Regular Inspections and Maintenance: Conducting frequent and thorough inspections allows for early detection of corrosion, enabling timely intervention and repair. Preventive maintenance strategies help address potential issues before they escalate.
- Corrosion Monitoring Systems: Implementing advanced sensors and monitoring systems enables continuous assessment of corrosion levels. These systems provide real-time data, facilitating informed decision-making and prompt corrective actions.

Impact on Airport Infrastructure

Airport infrastructure, primarily made of steel, is highly susceptible to corrosion, which weakens structures and thereby poses significant safety risks. Effective corrosion management is essential to prevent structural failures, accidents, and economic losses. For instance, maintaining the structural integrity of hangars where aircraft are maintained is crucial, as a roof collapse could result in significant damage to the aircraft housed within, leading to multi-million dollar losses for the airport, airlines, and maintenance companies.

Implementing a CHM system can significantly enhance the assurance of structural integrity through the deployment of appropriate sensors. These sensors facilitate continuous monitoring and early detection of potential issues, particularly corrosion, thereby aiding in timely maintenance and prevention of structural failures. For instance, installing an Acuity LS sensor kit on the structural beams of a hangar roof (Fig. 7.2), where corrosion is most likely to occur (Tzortzinis et al., 2020a), utilizing both painted and bare sensors, allows for a comprehensive assessment of the environmental conditions affecting the structure (Tzortzinis et al., 2020a, 2020b). This configuration enables the evaluation of the current state of the structure and the identification of potential future corrosion-related threats. By monitoring using corrosion sensors both coated and uncoated surfaces, the system can provide valuable data on the onset and progression of corrosion, facilitating proactive maintenance and ensuring structural integrity.

Figure 7.2. Example location of corrosion sensors on the hangar structure

Airport infrastructure includes comprises numerous metal structures, including hangars, control towers, bridges, and support frameworks. Steel is commonly used in

these structures, making them particularly vulnerable to atmospheric corrosion, which can lead to compromised structural integrity either in bare metal or in embedded steel in concrete. The corrosion in the former cause the reduction of load-bearing capacity; in the latter, the corrosion products generate spalling and weakening of the concrete, compromising the stability of the structure.

Corrosion-induced degradation of airport infrastructure poses significant safety risks. Structural failures can lead to accidents and operational disruptions, endangering lives and causing substantial economic losses. (Herzberg et al., 2019; United States Government Accountability Office, 2019). Ensuring the integrity of these structures through effective corrosion management is therefore mandatory, requiring frequent (the frequency of building inspections depends on the building regulations in a given country) inspections and maintenance activities, driving up operational costs. Preventive measures such as protective coatings and cathodic protection also contribute to the financial burden. Moreover, maintenance operations often lead to downtime and disruptions, affecting airport efficiency and reliability (Rakas et al., 2018).

Atmospheric corrosion is a pervasive and persistent challenge for the aviation industry, affecting both airport infrastructure and aircraft. The impacts of corrosion are far-reaching, encompassing structural integrity, safety, and operational efficiency. Through a combination of advanced materials, protective coatings, environmental controls, and proactive maintenance, the aviation industry can effectively manage and mitigate the risks associated with atmospheric corrosion. In particular, continued research and innovation in corrosion monitoring and prevention can be fundamental to learn how safeguarding the longevity and reliability of aviation assets.

Case Studies

To test the effectiveness of the CHM systems, two different locations in Italy were selected as corrosion test sites: the CNR-ICMATE facilities in Padua and Bonassola (MARECO Laboratory), shown in Fig. 7.3.

Figure 7.3. Two atmospheric corrosion test sites in Italy (CNR-ICMATE laboratories in Padua and Bonassola)

T he test site in Bonassola, a small village on the Ligurian coast of the Mediterranean Sea, is a sea-exposed site at MARECO, the CNR-ICMATE polythematic marine laboratory (Fig. 7.4). Here, a stand with sensors is placed on the balcony above a laboratory set inside a cave. During fall 2023, a severe storm induced particularly high surf, with waves causing intense washing of the Acuity LS position. In Padua the corrosion test site is located in an industrial zone, in the immediate vicinity of the highway (city bypass) and two large railway reloading facilities (Fig. 7.5). It is one of the most industrialized regions of northern Italy. These locations provide data from environments where aircraft and potential airport installations are most exposed to rapid corrosion.

Figure 7.4. View of the corrosion test station in Bonassola

Figure 7.5. View of the corrosion test station in Padua (Google view)

Sensors at both corrosion test sites were positioned similarly: one sensor was installed in an open-air environment, while the other was positioned inside an aircraft wingtip (simulating the microclimatic conditions within a confined space). An autonomous sensor array with an independent power supply, the Acuity LS (Fig. 7.6) from Luna Labs, was selected for this study (Friedersdorf et al., 2019). This choice was primarily influenced by the prior successful implementation of these sensors by AFIT in a flying helicopter in recent years, demonstrating their reliability and suitability for similar applications.

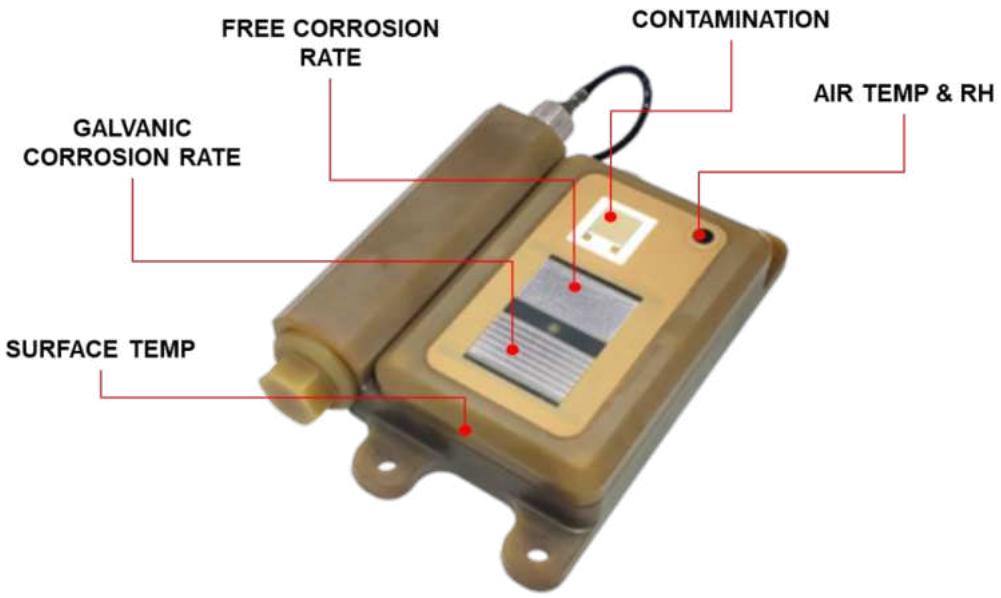

Figure 7.6. Acuity LS sensor system

Comprehensive measurements were taken for all parameters (presented in Table 7.1) every 30 minutes.

Table 7.1 Recording elements and registered parameters

Recording elements	**Registered parameters**
Air temperature (Ta)	-40ºC – +85ºC (±0.3%)
Relative humidity (RH)	0% – 100% (±2%)
Conductivity due to pollutants	micro-Siemens, µS
Free corrosion	Free corrosion current, µA Cumulative free corrosion, µC
Galvanic corrosion	Galvanic corrosion current, µA Cumulative galvanic corrosion, µC
Surface temperature (Ts)	-40ºC – +85ºC (±0.3%)

Acuity LS sensors output a conductivity measure in µS, due to pollutants such as SO_2 and NO_x, which can form acids in the presence of moisture, as well as C particles and chlorides. The free and galvanic corrosion outputs are measured in µA, the cumulative corrosion in µC, which is proportional to the mass loss rate of the sensor alloy in g/(m^2*year). These units are consistent with ISO 9223 standards for classifying, determining, and estimating the corrosivity of atmospheres. Corrosion

rate measurements are performed using laminated wafers produced from metals and engineering alloys. For testing, the sensors used the following metal combinations:

- for free corrosion measurements – aluminum 7075-T6;
- for galvanic corrosion measurements – a compilation of aluminum 7075-T6 and stainless steel A286.

Interestingly, after just 3 months, significant differences in the corrosivity of atmospheres were observed between the two corrosion test sites. Moreover, within the same site, the tests reveal appreciable differences in corrosivity between atmospheric corrosion (outside) and that observed inside a closed space (microclimate), shown in Figs. 7.7 and 7.8.

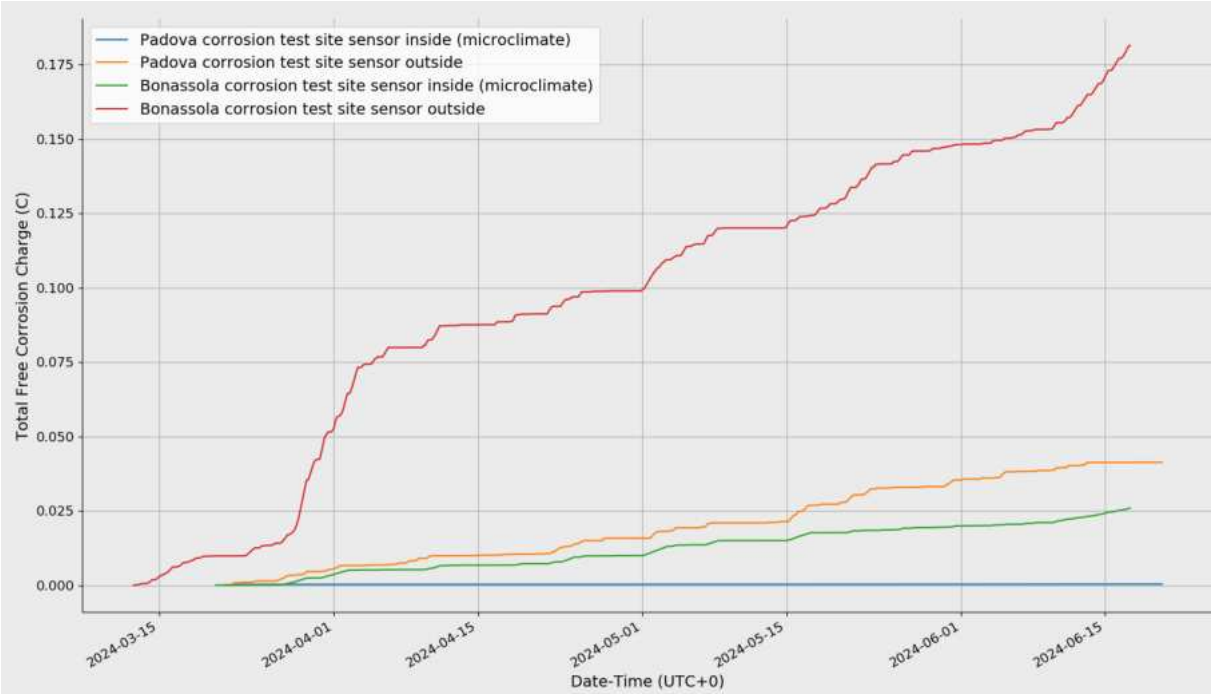

Figure 7.7. Total Free Corrosion Charge

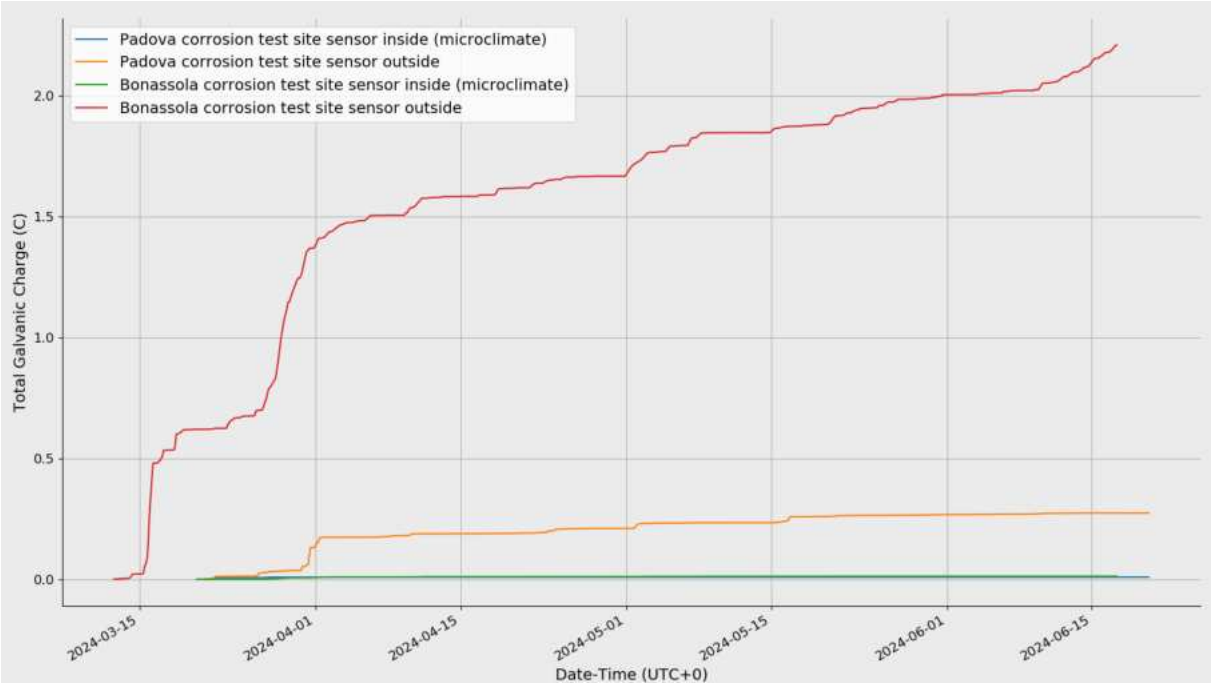

Figure 7.8. Total Galvanic Corrosion Charge

The microclimate within enclosed sections of aircraft wings involves specific environmental conditions present inside these structures, such as temperature, humidity, and the presence of chemicals or microorganisms. In aircraft wings composed of either metal or composite materials, temperature variations are significant and influenced by external conditions. At high altitudes, the external temperature can plummet to approximately -60°C, which directly impacts the internal temperature of the wings. Generally, the humidity within the wings is low, owing to the hermetic seal and the inherently low humidity of high-altitude air. Nevertheless, moisture ingress can occur through leaks or condensation, potentially leading to the corrosion of metallic components.

Figure 7.9 presents the chloride ingress into the internal structure of the wing, as evidenced by a delay of approximately 4 to 10 hours between the increase in conductance signals detected by the exterior and interior sensors. This delay indicates the time required for chloride ions to permeate from the wing's surface to its internal regions.

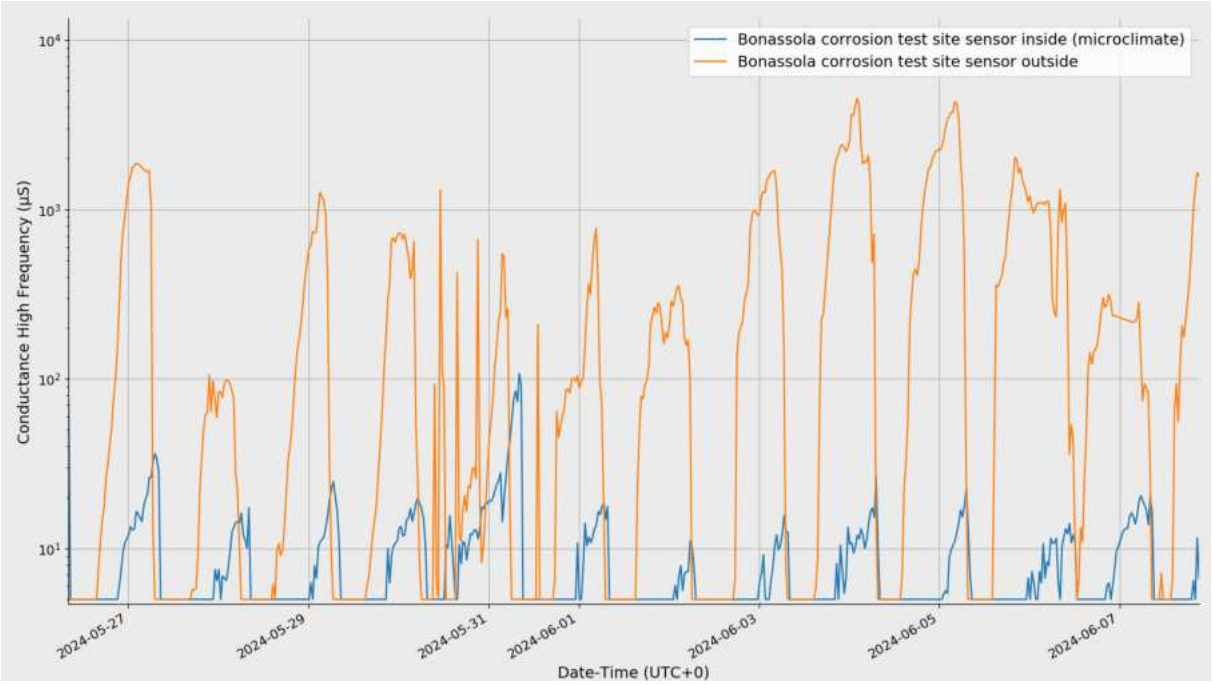

Figure 7.9. Conductance High Frequency

It is important to note that there may be various chemical substances inside the wings, such as lubricants, fuel (in the case of wings acting as fuel tanks), anti-corrosion agents and sealing materials. Although their presence and condition may influence the microclimate, they were excluded from this study in order to simplify the diagnostic models. Another aspect deliberately not included in the research is the measurement of the amount of air exchange, which may also affect moisture condensation and the accumulation of gases or chemical vapors. This decision was necessary to focus on the main microclimate conditions that would allow for determining climate corrosivity in accordance with the ISO 9223 standard.

This case study demonstrates the importance of environmental conditions in corrosion testing and the need for location-specific considerations when assessing material durability. The significant differences in corrosion rates seen between Padua and Bonassola underscore the role of sea water, particularly the high levels of chloride deposition recorded near the seaside. These results highlight the need for targeted protective measures and maintenance inspection based on data obtained during sensor measurements in environments with a) high chloride levels, b) common atmospheric pollutants, or c) both high chloride levels and atmospheric pollutants, the latter combination requiring intensive and targeted efforts to ensure the longevity of metallic structures and components.

Conclusions

This exploration of Condition Health Monitoring (CHM) systems has underscored their significant role in monitoring atmospheric corrosion and ensuring the structural integrity of aircraft. CHM systems provide a multi-faceted approach to enhancing aviation safety, optimizing maintenance procedures, and enabling data-driven decision-making.

The experimental campaign carried out at two different sites (Padua and Bonassola) using Acuity LS sensors demonstrated the capability of real-time corrosion monitoring. These results illustrate how CHM systems, when applied to aircraft, can support diagnostic and prognostic activity which leads to improved prevention of structural failures and ensure the safety of both passengers and crew. Furthermore, CHM systems enable a shift from reactive to proactive maintenance strategies, significantly lowering maintenance costs and enhancing the overall efficiency of airport operations.

The transformative impact of CHM systems on aviation safety and maintenance is profound. By leveraging advanced data analytics, these systems provide valuable insights that inform better maintenance planning and risk assessment. This leads to more informed decision-making, optimized resource allocation, and ultimately, a more reliable and efficient aviation industry.

Moving forward, it is crucial to encourage the further adoption and research of CHM systems. The benefits discussed herein highlight the significant advancements in safety, efficiency, and cost-effectiveness that these systems bring to aviation. However, realizing the full potential of CHM systems will require ongoing research and development to refine their capabilities and expand their applications.

References

Ciężak, P., & Rdzanek, A. (2020). Corrosion monitoring of aircraft based on the corrosion prognostic health management (CPHM) system. *Journal of KONBiN*, *50*(4), 205–216. https://doi.org/10.2478/jok-2020-0082

Cusati, V., Corcione, S., & Memmolo, V. (2021). Impact of structural health monitoring on aircraft operating costs by multidisciplinary analysis. *Sensors*, *21*(20), 6938. https://doi.org/10.3390/s21206938

Demo, J., Andrews, C., Friedersdorf, F., Morgan, A., & Jostes, L. (2013). Deployment of a wireless corrosion monitoring system for aircraft applications. *2013 IEEE Aerospace Conference,* Big Sky, MT, USA, 1–10. https://doi.org/10.1109/AERO.2013.6496924

Friedersdorf, F. J., Demo, J. C., Brown, N. K., & Kramer, P. C. (2019). Electrochemical sensors for continuous measurement of corrosion and coating system performance in outdoor and accelerated atmospheric tests. In S. Papavinasam, R. B. Rebak, L. Yang, & N. S. Berke (Eds.), *Advances in electrochemical techniques for corrosion monitoring and laboratory corrosion measurements* (pp. 91–113). ASTM International. https://doi.org/10.1520/stp160920170222

Herzberg, E., Acton, C., Chan, T., Guo, S., Lai, A., & Stroh, R. (2019). *Estimated impact of corrosion on cost and availability of DOD weapon systems – FY19 update*. LMI.

Hoen-Velterop, L. (2017). Assessing the corrosion environment severity helicopters encounter using environmental sensors. *Department of Defense – Allied Nations Technical Corrosion Conference*. Paper No. 2017-400177.

Li, L., Chakik, M., & Prakash, R. (2021). A review of corrosion in aircraft structures and graphene-based sensors for advanced corrosion monitoring. *Sensors*, *21*(9), 2908. https://doi.org/10.3390/s21092908

National Transportation Safety Board. (1988). *Aircraft accident report: Aloha Airlines Flight 243 (Boeing 737-200)* (Report No. PB89-910404). National Technical Information Service.

Rakas, J., Bauranov, A., & Messika, B. (2018). Failures of critical systems at airports: Impact on aircraft operations and safety. *Safety Science*, *110*, 141–157. https://doi.org/10.1016/j.ssci.2018.05.022

Tzortzinis, G., Knickle, B. T., Bardow, A., Breña, S. F., & Gerasimidis, S. (2020a). Strength evaluation of deteriorated girder ends. I: Experimental study on naturally

corroded I-beams. *Thin-Walled Structures*, 107220. https://doi.org/10.1016/j.tws.2020.107220

Tzortzinis, G., Knickle, B. T., Bardow, A., Breña, S. F., & Gerasimidis, S. (2020b). Strength evaluation of deteriorated girder ends. II: Numerical study on corroded I-beams. *Thin-Walled Structures*, 107216. https://doi.org/10.1016/j.tws.2020.107216

United States Government Accountability Office. (2019). *Defense Management: observations on changes to the reporting structure for DOD's corrosion office and its implementation of GAO recommendations* (Report to Congressional Committees, GAO-19-513). United States Government Accountability Office.

Wright, R. F., Lu, P., Devkota, J., Lu, F., Ziomek-Moroz, M., & Ohodnicki, P. R. (2019). Corrosion sensors for structural health monitoring of oil and natural gas infrastructure: A review. *Sensors*, *19*(18), 3964. https://doi.org/10.3390/s19183964

Contact: Patryk Ciężak - patryk.ciezak@wat.edu.pl